JL, Pestana A, et al. Allelic loss at 1p is associated with tumor progression of meningiomas. Genes Chromosomes Cancer 1994 : 9 ; 296-8.
31. Pfisterer WK, Hank NC, Preul MC, Hendricks WP, Pueschel J, Coons SW, et al. Diagnostic and prognostic significance of genetic regional heterogeneity in meningiomas. Neuro-oncol 2004 : 6 ; 290-9.
32. Weber RG, Bostrom J, Wolter M, Baudis M, Collins VP, Reifenberger G, et al. Analysis of genomic alterations in benign, atypical, and anaplastic meningiomas : toward a genetic model of meningioma progression. Proc Natl Acad Sci USA 1997 : 94 ; 1719-24.
33. Lamszus K, Kluwe L, Matschke J, Meissner H, Laas R, Westphal M. Allelic losses at 1p, 9q, 10q, 14q, and 22q in the progression of aggressive meningiomas and undifferentiated meningeal sarcomas. Cancer Genet Cytogenet 1999 : 110 ; 103-10.

Available online at www.sciencedirect.com

SCIENCE DIRECT®

Nuclear Medicine and Biology 33 (2006) 37–42

NUCLEAR MEDICINE — AND — BIOLOGY

www.elsevier.com/locate/nucmedbio

Reduced ^{125}I-*meta*-iodobenzylguanidine uptake and norepinephrine transporter density in the hearts of mice with MPTP-induced parkinsonism

Nobuyoshi Fukumitsu[a,*], Masahiko Suzuki[b], Takahiro Fukuda[c], Yasushi Kiyono[d], Satomi Kajiyama[e], Hideo Saji[e]

[a]*Proton Medical Research Center, University of Tsukuba, Tsukuba, Ibaragi 305-8575, Japan*
[b]*Department of Neurology, The Jikei University School of Medicine, Tokyo 105-8461, Japan*
[c]*Department of Neuroscience, Research Center of Medical Science, The Jikei University School of Medicine, Tokyo 105-8461, Japan*
[d]*Radioisotope Research Laboratory, Kyoto University Hospital, Kyoto 606-8501, Japan*
[e]*Department of Patho-Functional Bioanalysis, Graduate School of Pharmaceutical Sciences, Kyoto University, Kyoto 606-8561, Japan*

Received 4 June 2005; received in revised form 24 July 2005; accepted 26 July 2005

Abstract

Uptake of ^{123}I-*meta*-iodobenzylguanidine (^{123}I-MIBG) is markedly reduced in the hearts of patients with Parkinson's disease. Although the mechanism of this reduction is unclear, ^{125}I-MIBG uptake is similarly reduced in the hearts of mice with 1-methyl-4-phenyl-1,2,3,6-tetrahydroxypyridine (MPTP)-induced parkinsonism. Three groups of ten 15-week-old C57BL6 mice received intraperitoneal injections of (1) saline (control), (2) 10 mg/kg MPTP or (3) 40 mg/kg MPTP. After 0.185 MBq of ^{125}I-MIBG was injected, the percent injected dose of ^{125}I-MIBG per gram of tissue (%ID/g) was determined and cardiac concentrations of norepinephrine were measured. Cardiac concentrations of norepinephrine transporter (NET) were measured in three groups of twenty 15-week-old C57BL6 mice receiving these same treatments. The %ID/g in mice receiving 10 or 40 mg/kg MPTP (5.7±1.1 and 4.4±1.2%/g) was significantly lower than that in control mice (11.3±2.2%/g; $P<.00001$ and $P<.0000001$, respectively). The norepinephrine concentration in mice receiving 10 or 40 mg/kg MPTP ($7.86\pm0.67\times10^5$ and $7.50\pm0.89\times10^5$ pg/wet g) was significantly lower than that in control mice ($9.21\pm0.97\times10^5$ pg/wet g; $P<.01$ and $P<.001$, respectively). The NET density in mice receiving 10 or 40 mg/kg MPTP (81±12, 61±7 fmol/mg protein) was significantly lower than that in control mice (126±7 fmol/mg protein; $P<.000001$ and $P<.0000001$, respectively). The %ID/g of ^{125}I-MIBG and NET density decreased as the dose of MPTP increased. This study clearly shows that reduced cardiac ^{125}I-MIBG uptake in mice with MPTP-induced parkinsonism is closely related to the reduced NET density in postganglionic cardiac sympathetic nerve terminals.

Keywords: ^{125}I-*meta*-iodobenzylguanidine; Parkinson's disease; 1-Methyl-4-phenyl-1,2,3,6-tetrahydroxypyridine; Norepinephrine; Norepinephrine transporter

1. Introduction

Meta-iodobenzylguanidine (MIBG) is a physiological analogue of norepinephrine that is actively transported into norepinephrine granules of sympathetic nerve terminals by the norepinephrine transporter (NET) [1,2]. ^{123}I-MIBG is a radiolabeled MIBG that is used to evaluate myocardial sympathetic nerve damage in heart disease and to diagnose ischemic heart disease, cardiomyopathy and heart failure. Recently, ^{123}I-MIBG has been used to examine patients with autonomic dysfunction produced by neurodegenerative diseases, such as Parkinson's disease [3–5].

Parkinson's disease is usually diagnosed on the basis of clinical features, such as bradykinesia, resting tremor, rigidity and the response to levodopa. However, these features do not allow a definitive diagnosis in many patients, and follow-up examinations are often needed for confirmation. Specific markers that would help diagnose Parkinson's disease have not been found.

In patients with Parkinson's disease, sympathetic nerve dysfunction is present in both the central and peripheral nervous systems [6–8]. Therefore, cardiac sympathetic denervation, indicated by a marked reduction in cardiac ^{123}I-MIBG uptake, likely reflects systemic autonomic dysfunction. Although reduced cardiac ^{123}I-MIBG uptake is recognized as a specific finding of Parkinson's disease, clear correlations of cardiac ^{123}I-MIBG uptake with disease

* Corresponding author. Tel.: +81 29 853 7100; fax: +81 29 853 7102.
E-mail address: gzl13162@nifty.ne.jp (N. Fukumitsu).

0969-8051/$ – see front matter © 2006 Elsevier Inc. All rights reserved.
doi:10.1016/j.nucmedbio.2005.07.010

severity, duration and treatment effect, and the ability to differentiate Parkinson's disease from other neurodegenerative diseases have not been proven [5,9–13]. The main reason for this uncertainty is that the mechanism of reduced cardiac ^{123}I-MIBG uptake in Parkinson's disease remains unclear.

The neurotoxic chemical agent 1-methyl-4-phenyl-1,2,3,6-tetrahydroxypyridine (MPTP) produces symptoms resembling those of Parkinson's disease in humans and monkeys [14–16], and induces an almost complete, permanent and selective degeneration of nigrostriatal dopaminergic neurons in a specific strain of mice [17,18]. In addition, pretreatment of mice with MPTP significantly reduces cardiac ^{125}I-MIBG uptake [19], as is observed in patients with Parkinson's disease. Therefore, the MPTP-treated mouse is a useful model for investigating the mechanism of reduced cardiac ^{123}I-MIBG uptake in patients with Parkinson's disease.

Determining the mechanism of reduced cardiac ^{123}I-MIBG uptake in patients with Parkinson's disease would help clarify the mechanism of autonomic failure. Further developments of this research, such as measurements of ^{123}I-MIBG uptake and norepinephrine turnover in the heart and other organs with autonomic failure in patients with Parkinson's disease, would provide advanced information about foci of autonomic failure and lead to greater diagnostic accuracy and new drugs and treatments.

In this preclinical study, we investigated ^{125}I-MIBG uptake and norepinephrine turnover in the hearts of Parkinson's disease model mice treated with MPTP.

2. Materials and methods

All experiments were done in accordance with the "Principles of Laboratory Animal Care" (NIH publication no. 86-23, revised 1985).

2.1. Cardiac ^{125}I-MIBG uptake and concentrations of norepinephrine

Thirty 15-week-old C57BL6 mice were used to establish an experimental model of Parkinson's disease. The mice were fed standard laboratory chow and given free access to water. They were divided into three groups of 10 mice each, which received intraperitoneal injections of (1) saline (control), (2) 10 mg/kg MPTP (Sigma-Aldrich, St. Louis, MO; dissolved in 0.9% saline, one injection) or (3) 40 mg/kg MPTP (divided into four injections given at 12-h intervals).

Seven days after the last injection of saline or MPTP, 0.185 MBq of ^{125}I-MIBG (Daiichi Radioisotope Laboratories, Tokyo, Japan) with a specific activity of 9.25 MBq (0.25 mCi) per milligram was injected through a lateral tail vein. The mice were killed by cervical dislocation 4 h later. The hearts were immediately dissected and weighed. The percent injected dose per gram of tissue (%ID/g) of ^{125}I-MIBG in the heart was measured.

The concentrations of norepinephrine in the heart were measured. A mixture of 0.6 ml of heart tissue and 0.3 ml of deproteinization solution (6% perchloric acid solution/3.5 M sodium acetate, 5:1 v/v) was stirred and centrifuged (1200×*g*) at 4°C for 15 min. The clear supernatant was applied to an autosampler of a high-performance liquid chromatographic (HPLC) analyzer.

After 250 μl of the supernatant was automatically injected into the analyzer, concentrations of free catecholamines (CAs) were measured with the HPLC analyzer. With a microprocessor-controlled column-switching device, each sample was delivered to a pre-column (TSK pre-column CA1 7.5×7.5 mm, Tosoh, Tokyo, Japan) equilibrated with eluent A (0.06 M sodium acetate, anhydrous buffer containing 4.8% acetonitrile). The pass fraction was delivered to another pre-column (TSK pre-column CA2 4×60 mm, Tosoh) equilibrated with the same eluent A. Absorbed CAs were eluted with eluent B (0.32 M ammonium nitrate buffer) and delivered to an analytical column (Wacosil-II 5C18RS 4.6×150 mm, Wako Industries, Osaka, Japan) equilibrated with the same eluent B. Each separated CA was delivered to a reaction coil (60°C) with fluorogenic reagent C (diphenylethylenediamine in a 50% ethanol solution) and converted to diphenylethylenediamine derivatives. The fluorescent intensity of each eluate from the reaction unit was measured in a detector at a wavelength of 483 nm with an excitation wavelength of 347 nm [20].

2.2. Binding assay for cardiac NET

Sixty 15-week-old C57BL6 mice were divided into three groups of 20 mice that received intraperitoneal injections of (1) saline (control), (2) 10 mg/kg MPTP or (3) 40 mg/kg MPTP. Seven days after the last injections of MPTP, the mice were killed and their hearts were immediately dissected and weighed. The concentration of the NET, whose function is norepinephrine reuptake, was measured. Membrane preparations for binding assays were made as described previously [21,22]. Mouse hearts were homogenized in 20 volumes of ice-cold 250 mM sucrose buffer (5 mM Tris, 1 mM $MgCl_2$, 250 mM sucrose) with a 30-s burst in a homogenizer (Kinematica Polytron PT 10/35, Brinkmann Instruments, Westbury, NY, USA) set at speed 6. Homogenates were centrifuged at 750×*g* for 10 min. The pellets were discarded and the supernatant was recentrifuged at 20,000×*g* for 20 min. The resulting pellets were resuspended in 10 volumes of ice-cold 50 mM Tris–HCl buffer (50 mM Tris, 5 mM KCl, and 120 mM NaCl, pH 7.4) and recentrifuged to obtain a pellet. Pellets thus obtained were resuspended in 5 volumes of Tris–HCl buffer and stored at −80°C until use. Protein concentrations were measured with the method of Lowry [23].

Binding assays were performed as described previously with some minor modifications [21,22]. Briefly, [^{3}H]desipramine binding was determined by incubating aliquots of membrane suspension with [^{3}H]desipramine (0.25–0.30 nM) in a final volume of 250 μl for 30 min at 25°C. The binding

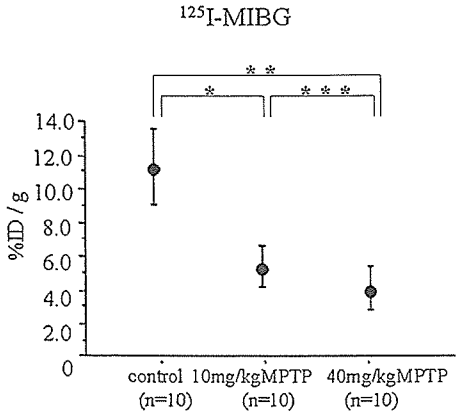

Fig. 1. ^{125}I-MIBG uptake. The %ID/g of the 10-mg/kg MPTP group was significantly lower than that of the control group, and that of the 40-mg/kg MPTP group was significantly lower than those of the control and the 10-mg/kg MPTP groups. *P<.00001, **P<.0000001, ***P<.05.

was terminated by diluting the incubation mixture with 5 ml of ice-cold 50 mM Tris–HCl buffer (pH 7.4) and filtration through glass microfiber filters (GF/B, Whatman, Maidstone, Kent, UK) with a 24-channel cell harvester (M-24, Brandel, Gaithersburg, MD, USA). Finally, each filter was rinsed three times with 5 ml of ice-cold 50 mM Tris–HCl buffer (pH 7.4). The radioactivity on the filters was determined with a liquid scintillation counter (Tri-Carb 2500-TR Liquid Scintillation Analyzer, Packard BioScience, Meridian, CT). Nonspecific binding was defined with 100 μM nisoxetine. The equilibrium dissociation affinity constants (K_D) and the maximal specific binding (B_{max}) were calculated from specific binding values by Scatchard analyses.

The data are expressed as mean values±standard values. All results were analyzed by one-factor analysis of variance and Welch's t test, and raw P values were adjusted with the Bonferroni/Dunn correction for intergroup comparisons, that is, adjusted P values were calculated as raw P value× (the number of groups−1) [24]. An adjusted P value <.05 was considered to indicate statistical significance.

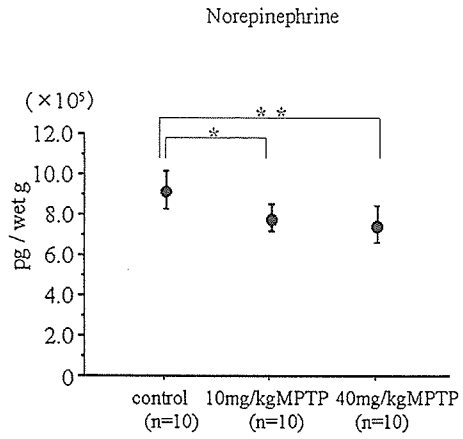

Fig. 2. Norepinephrine concentration. The norepinephrine concentrations of the 10- and 40-mg/kg MPTP groups were significantly lower than that of the control group. *P<.01, **P<.001.

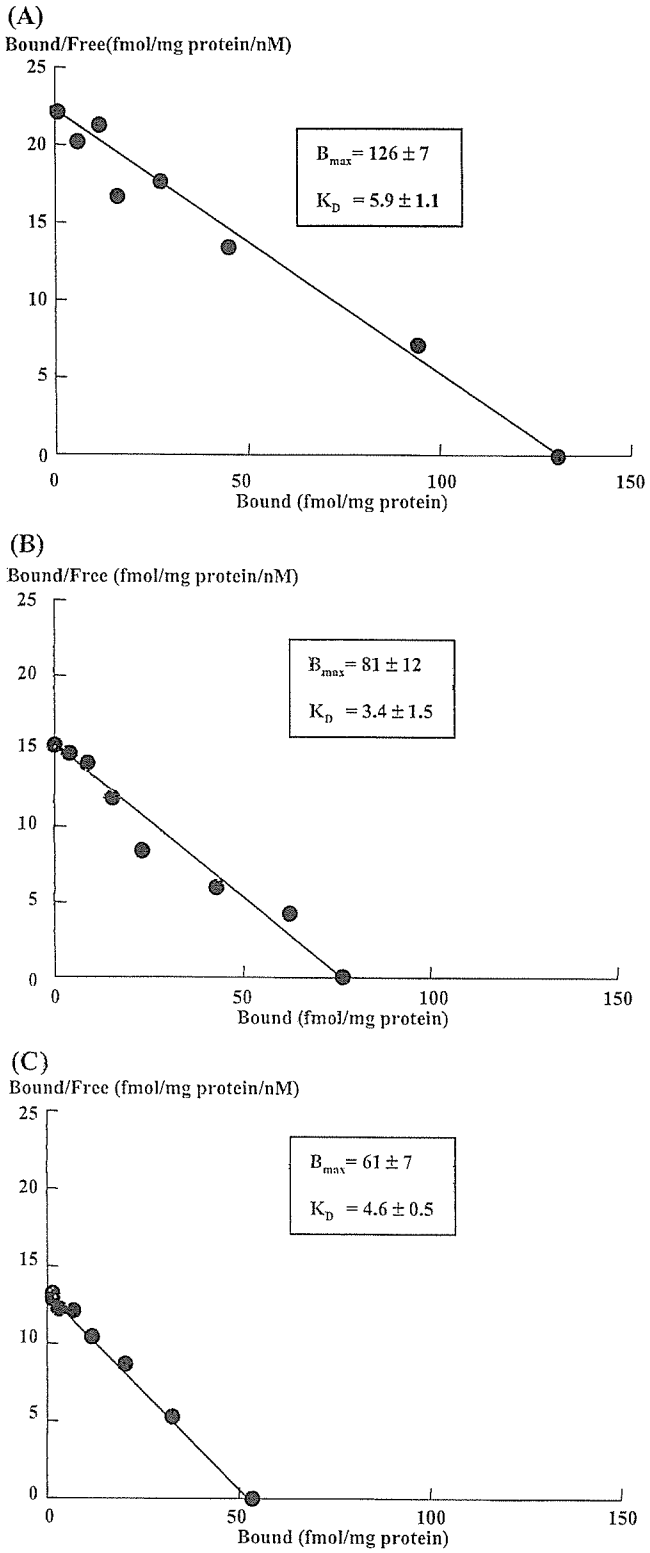

Fig. 3. NET density (A) control, (B) MPTP 10 mg/kg, (C) MPTP 40 mg/kg. Scatchard plots of three typical experiments. The equilibrium dissociation affinity constants (K_D) and the maximal specific binding (B_{max}) were calculated by Scatchard analysis. The NET B_{max} of the 10 mg/kg MPTP group was significantly lower than that of the control group (P<.000001), and that of the 40-mg/kg MPTP group was significantly lower than those of the control (P<.0000001) and the 10-mg/kg MPTP groups (P<.001).

3. Results

3.1. ^{125}I-MIBG uptake

The %ID/g of the 10-mg/kg MPTP group was significantly lower than that of the control group (5.7±1.1% vs. 11.3±2.2%/g, $P<.00001$). The %ID/g of the 40-mg/kg MPTP group (4.4±1.2%/g) was significantly lower than that of the control group ($P<.0000001$) and that of the 10-mg/kg MPTP group ($P<.05$). The %ID/g decreased as the dose of MPTP increased (Fig. 1).

3.2. Norepinephrine concentration

The norepinephrine concentrations of the 10-mg/kg MPTP group ($7.86\pm0.67\times10^5$ pg/wet g) and the 40-mg/kg MPTP group ($7.50\pm0.89\times10^5$ pg/wet g) were significantly lower than that of the control group ($9.21\pm0.97\times10^5$ pg/wet g, $P<.01$ and $P<.001$, respectively, Fig. 2).

3.3. NET density

The NET density of the 10-mg/kg MPTP group was significantly lower than that of the control group (81±12 vs. 126±7 fmol/mg protein, $P<.000001$). The NET density of the 40-mg/kg MPTP group (61±7 fmol/mg protein) was significantly lower than that of the control group ($P<.0000001$) and that of the 10-mg/kg MPTP group ($P<.001$). The NET density decreased as the dose of MPTP increased (Fig. 3).

4. Discussion

Neurological effects following systemic application of MPTP have been found in a variety of animals, including monkeys, mice, dogs, cats, sheep and even goldfish [14–16,25–27]. Mice treated with MPTP show initial acute toxic effects of decreased locomotor activity, mydriasis, pilorection, hypersalivation and clonic seizures [28,29]. The mechanism of MPTP neurotoxicity involves several steps. In the first step, MPTP, which readily enters the brain, is converted, possibly in the glia, by MAO-B to MPP^+, the likely ultimate toxic agent. The second step is a fairly selective uptake of MPP^+ by dopaminergic terminals in the striatum via the monoamine transporter and subsequent intraterminal vesicular storage [26,27]. Autonomic dysfunction in the cardiovascular system, such as the MPTP-dose-related decrease in mean arterial blood pressure, has been reported in rats [30]. Selective inhibition by MPP^+ of complex I activity in cardiac mitochondria is considered to be an important cause of nerve degeneration in the heart. However, this theory remains unproven, and other factors may be involved in MPTP neurotoxicity in the heart.

The C57BL6 mouse has been used in many studies of parkinsonism [14–16]. This mouse is highly sensitive to MPTP, which induces dose-dependent neurotoxic effects [28,31–33]. Takatsu et al. [19] have reported that treatment with 5, 10 and 100 mg/kg MPTP significantly reduces cardiac ^{125}I-MIBG uptake in C57BL6 mice. Our first experimental protocol used the method of Takatsu et al. However, because several mice died within a few days of receiving MPTP, we revised the protocol to use the method of Marien et al. [33], which produced a 40% decrease in dopamine with a dose of 40 mg/kg MPTP. The MPTP-dose-dependent reduction in cardiac ^{125}I-MIBG uptake reported by Takatsu et al. suggested that a dose of 40 mg/kg MPTP would be appropriate for establishing a murine model of severe Parkinson's disease. Although the neurotoxic effects of MPTP are dose-dependent, the effects naturally differ between individuals. To minimize the effect of individual differences, we measured cardiac ^{125}I-MIBG uptake and norepinephrine concentration in three groups of 10 mice and performed binding assays for cardiac NET density in three groups of 20 mice.

We found that the cardiac NET density in MPTP-treated C57BL6 mice decreased dose dependently in a manner similar to cardiac ^{125}I-MIBG uptake. Because ^{125}I-MIBG is actively transported into norepinephrine granules of sympathetic nerve terminals by NET, this result indicates that the mechanism of the reduced cardiac ^{125}I-MIBG uptake in mice with MPTP-induced parkinsonism is a reduction in cardiac NET density. The manner in which cardiac NET density decreased was slightly different from that of the cardiac norepinephrine concentration, that is, the cardiac NET density was significantly lower in the 40-mg/kg MPTP group than in the 10-mg/kg group. In contrast, cardiac norepinephrine concentrations did not differ significantly between these groups. We found that the cardiac norepinephrine concentration in mice treated with 10 or 40 mg/kg MPTP decreased to 85.3% and 81.3%, respectively, of that in control mice. This finding suggests that even if the MPTP dose is markedly increased, the cardiac norepinephrine concentration would reach a plateau of approximately 80% of the level in untreated mice. Eisenhofer et al. [34] have reported that most of the norepinephrine released from vesicles at the sympathetic nerve terminal is taken up again by sympathetic nerves; the axoplasmic norepinephrine is either sequestered into vesicles or metabolized to dihydroxyphenylglycol in the normal human heart at rest. Axoplasmic norepinephrine represents 90% of the norepinephrine leaked from vesicles in the healthy human heart. A small amount of norepinephrine, 10% of that leaked from vesicles, is released by sympathetic nerves, taken up again via Uptake 1, and sequestered from the axoplasm into storage vesicles. We have postulated the following mechanisms to explain why the norepinephrine concentrations of the 10- and 40-mg/kg MPTP group were not significantly different, despite the cardiac NET density of the two groups being significantly different. Recaptured norepinephrine in the hearts of 10 mg/kg MPTP group was severely diminished and reached at most the level at which little norepinephrine was taken up because of the reduced cardiac NET density. The axoplasmic norepinephrine, which was not affected by NET and circulated in the nerve terminal, comprised most of the

norepinephrine leaked from vesicles. These suggested mechanisms explain, we believe, why the difference in recaptured norepinephrine between the 10- and 40-mg/kg MPTP groups was slight and not statistically significant. A further study, for example, multipoints analysis of norepinephrine and ^{125}I-MIBG uptake to the same time scale after administration of MPTP, should give us more detailed information about the mechanism of reduced ^{125}I-MIBG uptake in the heart.

Some studies have attempted to clarify the mechanism of the reduced cardiac ^{123}I-MIBG uptake in patients with Parkinson's disease. Takatsu et al. [35] have found in their in vitro and in vivo studies with an MPTP-treated pheochromocytoma cell line that MPTP affects mainly the neuronal part of ^{125}I-MIBG uptake, indicating sympathetic impairment in the hearts of MPTP-pretreated mice. They have also shown that MPTP directly impairs active uptake of MIBG and that the marked decrease in MIBG uptake is caused by dysfunction of sympathetic nerve endings, not by acute cell death or secondary impairment of sympathetic nerve cells. Orimo et al. [36,37] have reported that tyrosine hydroxylase (TH)-immunoreactive fibers are markedly decreased in the hearts of patients with Parkinson's disease examined at autopsy, and that the decrease in TH is clearly coincident with the reduced ^{123}I-MIBG uptake. Decreases in TH have also been shown, with immunocytochemical analyses using antibodies against TH, in the substantia nigra and the ventral tegmental area of MPTP-treated C57BL6 mice [38,39]. Although systemic investigations have not been done in MPTP-treated mice, the decrease in TH has been proposed as a possible mechanism of the reduced cardiac ^{125}I-MIBG uptake in the hearts of mice with MPTP-induced parkinsonism.

However, we have found that the MPTP-dose-dependent decrease in cardiac NET density was similar to the decrease in cardiac ^{125}I-MIBG uptake and was greater than the decrease in the cardiac norepinephrine concentration, suggesting that reduced cardiac ^{125}I-MIBG uptake was equal to or more affected by cardiac NET density than TH. We agree that damage to postganglionic sympathetic nerves decreases cardiac ^{125}I-MIBG uptake. In addition, the results of our study clearly show that the reduced cardiac ^{125}I-MIBG uptake in mice with MPTP-induced parkinsonism is closely related to the reduced cardiac NET density in postganglionic cardiac sympathetic nerve terminals.

5. Conclusion

^{125}I-MIBG uptake and NET density are MPTP dose dependently decreased in the hearts of mice with MPTP-induced parkinsonism.

Acknowledgment

We are grateful to Daiichi Radioisotope Laboratories, Tokyo, Japan, for supplying ^{125}I-MIBG and to SRL, Tokyo, Japan, for assaying catecholamines. We are also grateful to Satoshi Orimo for his helpful advice.

References

[1] Wieland DM, Brown LE, Rogers WL, Worthington KC, Wu JL, Clinthorne NH, et al. Myocardial imaging with a radioiodinated norepinephrine storage analogue. J Nucl Med 1981;22:22–31.

[2] Glowniak JV, Kilty JE, Amara SG, Hoffman BJ, Turner FE. Evaluation of metaiodobenzylguanidine uptake by the norepinephrine, dopamine and serotonin transporters. J Nucl Med 1993;34: 1140–6.

[3] Yoshita M, Hayashi M, Hirai S. Decreased myocardial accumulation of ^{123}I-metaiodobenzyl guanidine in Parkinson's disease. Nucl Med Commun 1998;19:137–42.

[4] Orimo S, Ozawa E, Nakade S, Sugimoto T, Mizusawa H. ^{123}I-metaiodobenzylguanidine myocardial scintigraphy in Parkinson's disease. J Neurol Neurosurg Psychiatry 1999;67:189–94.

[5] Satoh A, Serita T, Seto M, Tomita I, Satoh H, Iwanaga K, et al. Loss of ^{123}I-MIBG uptake by the heart in Parkinson's disease: assessment of cardiac sympathetic denervation and diagnostic value. J Nucl Med 1999;40:371–5.

[6] Linden D, Diehl RR, Berlit P. Sympathetic cardiovascular dysfunction in long-standing idiopathic Parkinson's disease. Clin Auton Res 1997;7:311–4.

[7] Wakabayashi K, Takahashi H. Neuropathology of autonomic nervous system in Parkinson's disease. Eur Neurol 1997;38:2–7.

[8] Goldstein DS. Dysautonomia in Parkinson's disease: neurocardiological abnormalities. Lancet Neurol 2003;2:669–76.

[9] Braune S, Reinhardt M, Schnitzer R, Riedel A, Lucking CH. Cardiac uptake of [^{123}I]MIBG separates Parkinson's disease from multiple system atrophy. Neurology 1999;53:1020–5.

[10] Takatsu H, Nagashima K, Murase M, Fujiwara H, Nishida H, Matsuo H, et al. Differentiation of Parkinson disease from multiple-system atrophy measuring cardiac iodine-123 metaiodobenzylguanidine accumulation. JAMA 2000;284:44–5.

[11] Taki J, Nakajima K, Hwang EH, Matsunari I, Komai K, Yoshita M, et al. Peripheral sympathetic dysfunction in patients with Parkinson's disease without autonomic failure is heart selective and disease specific. Eur J Nucl Med 2000;27:566–73.

[12] Hamada K, Hirayama M, Watanabe H, Kobayashi R, Ito H, Ieda T, et al. Onset age and severity of motor impairment are associated with reduction of myocardial ^{123}I-MIBG uptake in Parkinson's disease. J Neurol Neurosurg Psychiatry 2003;74:423–6.

[13] Akincioglu C, Unlu M, Tunc T. Cardiac innervation and clinical correlates in idiopathic Parkinson's disease. Nucl Med Commun 2003;24:267–71.

[14] Langston JW, Ballard P, Tetrud JW, Irwin I. Chronic parkinsonism in human due to a product of meperidine-analog synthesis. Science 1982;219:979–80.

[15] Burns RS, Vhiueh CC, Markey SP, Ebert MH, Javobowitz DM, Kopin IJ. A primate model of parkinsonism: selective destruction of dopaminergic neurons in the pars compacta of the substantia nigra by *N*-methyl-4-phenyl-1,2,3,6-tetrahydroxypyridine. Proc Natl Acad Sci U S A 1983;80:4546–50.

[16] Heikkila RE, Sonsalla PK. The MPTP-treated mouse as a model of parkinsonism: how good is it? Neurochem Int 1992;20(Suppl): 299S–303S.

[17] Sundstrom E, Stromberg I, Tsutsumi T, Olson L, Jonsson G. Studies on the effect of 1-methyl-4-phenyl-1,2,3,6-tetrahydroxypyridine (MPTP) on central catecholamine neurons in C57 BL/6 mice. Comparison with three other strains of mice. Brain Res 1987;405: 26–38.

[18] Sonsalla PK, Heikkila RE. The influence of dose and dosing interval on MPTP-induced dopaminergic neurotoxicity in mice. Eur J Pharmacol 1986;129:339–45.

[19] Takatsu H, Nishida H, Matsuo H, Watanabe S, Nagashima K, Wada H, et al. Cardiac sympathetic denervation from the early stage of Parkinson's disease — clinical and experimental studies with radiolabelled MIBG. J Nucl Med 2000;41:71–7.

[20] Yoshimura M, Komori T, Nakanishi T, Takanashi H. Estimation of sulphoconjugated catecholamine concentrations in plasma by high-performance liquid chromatography. Ann Clin Biochem 1993;30: 135–41.

[21] Kiyono Y, Iida Y, Kawashima H, Tamaki N, Nishimura H, Saji H. Regional alterations of myocardial norepinephrine transporter density in streptozotocin-induced diabetic rats: implications for heterogeneous cardiac accumulation of MIBG in diabetes. Eur J Nucl Med 2001; 28:894–9.

[22] Kiyono Y, Iida Y, Kawashima H, Ogawa M, Tamaki N, Nishimura H, et al. Norepinephrine transporter density as a causative factor in alterations in MIBG myocardial uptake in NIDDM model rats. Eur J Nucl Med Mol Imaging 2002;29:999–1005.

[23] Lowry OH, Rosebrough NJ, Farr AL, Randall RJ. Protein measurements with the Folin phenol reagent. J Biol Chem 1951;193:265–75.

[24] Hochberg Y, Tamhane AC. Multiple comparison procedures. New York: Wiley Series in Probability and Mathematical Statistics; 1987.

[25] Zigmond MJ, Stricker EM. Animal models of parkinsonism using selective neurotoxins: clinical and basic implications. In: Smythies JR, Bradley RJ, editors. International review of neurobiology, vol. 31. San Diego: Academic Press; 1989. p. 10–79.

[26] Gerlach M, Riederer P, Przuntek H, Youdim MB. MPTP mechanisms of neurotoxicity and their implications for Parkinson's disease. Eur J Pharmacol 1991;208:273–86.

[27] Tipton KF, Singer TP. Advances in our understanding of the mechanisms of the neurotoxicity of MPTP and related compounds. J Neurochem 1993;61:1191–206.

[28] Sundström E, Fredriksson A, Archer T. Chronic neurochemical and behavioral changes in MPTP-lesioned C57BL/6 mice: a model for Parkinson's disease. Brain Res 1990;528:181–8.

[29] Zuddas A, Vaglini F, Fornai F, Corsini GU. Selective lesion of the nigrostriatal dopaminergic pathway by MPTP and acetaldehyde or diethyldithiocarbamate. Neurochem Int 1992;20(Suppl):287S–93S.

[30] Fuller RW, Hahn RA, Snoddy HD, Wikel JH. Depletion of cardiac norepinephrine in rats and mice by 1-methyl-4-phenyl-1,2,3, 6-tetrahydropyridine (MPTP). Biochem Pharmacol 1984;33:2957–60.

[31] Ricaurte GA, Langston JW, Delanney LE, Irwin I, Peroutka SJ, Forno LS. Fate of nigrostriatal neurons in young mature mice given 1-methyl-4-phenyl-1,2,3,6-tetrahydropyridine: a neurochemical and morphological reassessment. Brain Res 1986;376:117–24.

[32] Heikkila RE, Sieber BA, Manzino L, Sonsalla PK. Some features of the nigrostriatal dopaminergic neurotoxin 1-methyl-4-phenyl-1,2,3,6-tetrahydropyridine (MPTP) in the mouse. Mol Chem Neuropathol 1989;10:171–83.

[33] Marien M, Briley M, Colpaert F. Noradrenaline depletion exacerbates MPTP-induced striatal dopamine loss in mice. Eur J Pharmacol 1993;236:487–9.

[34] Eisenhofer G, Esler MD, Meredith IT, Dart A, Cannon III RO, Quyyumi AA, et al. Sympathetic nervous function in human heart as assessed by cardiac spillovers of dihydroxyphenylglycol and norepinephrine. Circulation 1992;85:1775–85.

[35] Takatsu H, Wada H, Maekawa N, Takemura M, Saito K, Fujiwara H. Significant reduction of ^{125}I-meta-iodobenzylguanidine accumulation directly caused by 1-methyl-4-phenyl-1,2,3,6-tetrahydroxypyridine, a toxic agent for inducing experimental Parkinson's disease. Nucl Med Commun 2002;23:161–6.

[36] Orimo S, Oka T, Miura H, Tsuchiya K, Mori F, Wakabayashi K, et al. Sympathetic cardiac denervation in Parkinson's disease and pure autonomic failure but not in multiple system atrophy. J Neurol Neurosurg Psychiatry 2002;73:776–7.

[37] Orimo S, Ozawa E, Nakade S, Hattori H, Tsuchiya K, Taki K, et al. [^{123}I] meta-iodobenzylguanidine myocardial scintigraphy differentiates corticobasal degeneration from Parkinson's disease. Intern Med 2003;42:127–8.

[38] Date I, Felten DL, Felten SY. Long-term effect of MPTP in the mouse brain in relation to aging: neurochemical and immunocytochemical analysis. Brain Res 1990;519:266–76.

[39] Kupsch A, Loschmann PA, Sauer H, Arnold G, Renner P, Pufal D, et al. Do NMDA receptor antagonists protect against MPTP-toxicity? Biochemical and immunocytochemical analyses in black mice. Brain Res 1992;592:74–83.

WILEY InterScience® DISCOVER SOMETHING GREAT

Journal of Neuroscience Research 84:1350–1357 (2006)

Decline of Striatal Dopamine Release in Parkin-Deficient Mice Shown by Ex Vivo Autoradiography

Shigeto Sato,[1,2] Tomoki Chiba,[2] Shingo Nishiyama,[3] Takeharu Kakiuchi,[3] Hideo Tsukada,[3] Taku Hatano,[1] Takahiro Fukuda,[4] Yasunobu Yasoshima,[5] Nobuyuki Kai,[5] Kazuto Kobayashi,[5] Yoshikuni Mizuno,[1] Keiji Tanaka,[2] and Nobutaka Hattori[1]*

[1]Department of Neurology, Juntendo University School of Medicine, Bunkyo, Tokyo, Japan
[2]Tokyo Metropolitan Institute of Medical Science, Bunkyo, Japan
[3]Central Research Laboratory, Hamamatsu Photonics K.K., Hamamatsu, Shizuoka, Japan
[4]Division of Neuropathology, Department of Neuroscience, Research Center for Medical Sciences, The Jikei University School of Medicine, Minato-ku, Tokyo, Japan
[5]Department of Molecular Genetics, Institute of Biomedical Sciences, School of Medicine, Fukushima Medical University, Fukushima, Japan

Parkin is the causal gene of autosomal recessive juvenile parkinsonism (AR-JP). Dopamine (DA) metabolism has been linked to Parkinson's disease (PD). To understand the pathogenesis of AR-JP, we generated parkin-deficient mice to assess the status of DA signaling pathway and examine DA release and DA receptor by ex vivo autoradiography. Ex vivo autoradiography using [^{11}C]raclopride showed a clear decrease in endogenous DA release after methamphetamine challenge in parkin-deficient mice. Furthermore, parkin deficiency was associated with considerable upregulation of DA (D_1 and D_2) receptor binding in vivo in the striatum and increased DA levels in the midbrain. Our results suggest that dopaminergic neurons could behave abnormally before neuronal death.

Key words: parkin; dopamine; release; autoradiography; receptor

Parkinson's disease (PD) is the most common neurodegenerative movement disorder in the elderly and affects approximately 1% of the population >65 years of age. The major symptoms of PD are tremor, bradykinesia, cogwheel rigidity, and postural instability, which arise from the degeneration of dopaminergic (DAergic) neurons in the substantia nigra (SN). Of the many hereditary PD genes, the *parkin* gene has received special interest by researchers working in the field of PD (Kitada et al., 1998), because it displays ubiquitin-ligase activity and that early investigations showed that proteolytic dysfunction causes massive loss of DAergic neurons (Shimura et al., 2000; Chung et al., 2001; Imai et al., 2001). Several lines of parkin-null mice have been generated, however, the mechanism(s) underlying the cause of autosomal-recessive-juvenile-parkinsonism (AR-JP) are less well defined, because most (if not all) substrates for parkin reported so far remain unchanged irrespective of parkin-deficiency (our unpublished results) (Goldberg et al., 2003; Periquet et al., 2005). The aim of the present study was to uncover the pathogenesis of AR-JP using parkin-deficient mice.

Imaging of changes in neuroreceptor availability to positron emission tomography (PET) ligands can be used to indirectly measure synaptic neurotransmitter fluxes in the living human brain and several PET studies in PD have been reported (Dagher, 2001; de la Fuente-Fernandez and Stoessl, 2002). In PD, the characteristic loss of striatal dopamine (DA) terminal function, reflected by reduced dopa decarboxylase activity, can be quantified in vivo using [^{18}F]dopa PET. Although striatal [^{18}F]dopa uptake reflects the storage of DA, [^{11}C]raclopride, an in vivo marker of dopamine D_2 receptor, is useful for assessing the capacity of endogenous DA release (Piccini et al., 2003). We monitored the status of DA metabolism in the brains of parkin-null mice, and focused on DA release and DA receptor by using ex vivo autoradiography techniques.

MATERIALS AND METHODS

Generation of Parkin$^{-/-}$ Mice

For the constructed targeting vector, most of exon 2 was replaced in-frame by the coding sequence of τ-GFP to

*Correspondence to: Nobutaka Hattori, MD, PhD, Department of Neurology, Juntendo University School of Medicine, 2-1-1 Hongo, Bunkyo, Tokyo, Japan. E-mail: nhattori@med.juntendo.ac.jp

Received 5 February 2006; Revised 25 May 2006; Accepted 29 June 2006

Published online 29 August 2006 in Wiley InterScience (www.interscience.wiley.com). DOI: 10.1002/jnr.21032

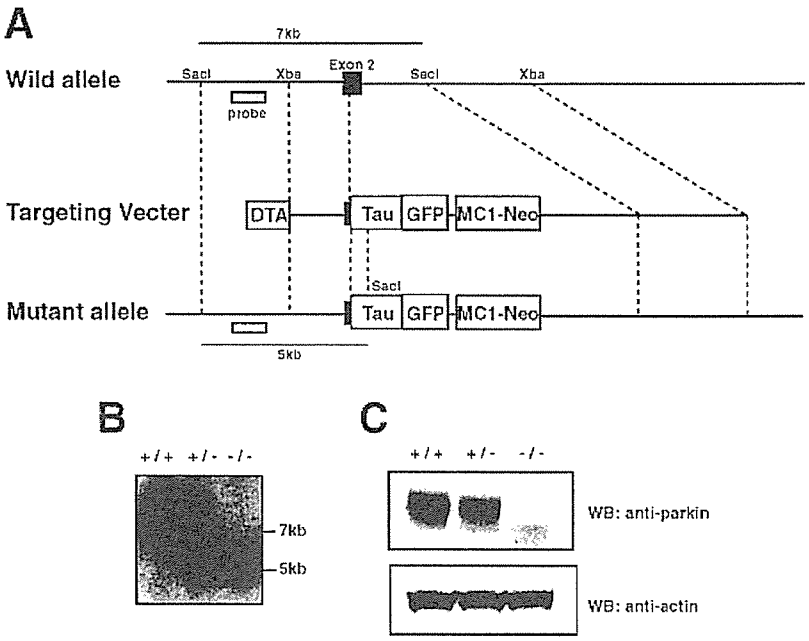

Fig. 1. Generation of parkin-deficient mice. **A:** Schematic representation of the targeting vector and the targeted allele of *parkin* gene. Exon 2 is depicted by the black box. The τ, GFP, MC1-Neo (neomycin-resistant) gene cassette is shown. The probe for Southern blot analysis is shown as a gray square. DTA, diphtheria toxin gene. **B:** Southern blot analysis of genomic DNAs extracted from tails of wild-type (+/+), heterozygous (+/−) or homozygous (−/−) mice. The genomic DNAs digested with *SacI* were hybridized with the probe shown in (A). Wild-type and mutant alleles are detected as 7- and 5-kb bands, respectively. **C:** Western blotting of parkin in whole brain lysates. The lysates of mice indicated genotypes were immunoblotted with antibodies against parkin and actin.

use as a reporter system for axonal extension, followed by translation and transcription termination sequences and the MC1-neo cassette (Fig. 1A). A targeting vector was constructed using 1.5- and 7-kb DNA fragments as 5′ and 3′ homologous sequences, respectively. A negative selection cassette, DTA, which encodes the diphtheria toxin, was also included. The linearized targeting vector was transfected into TT2 ES cells. After selection in G418, clones were screened by Southern analysis for homologous recombination. Using the 5′ external probe and probe specific for Neo sequence, we confirmed the clones carried the desired homologous recombination. ES cells of clones were injected into C57BL/6J. Chimeric offspring were crossed with C57BL/6J mice to obtain germline transmission, which was confirmed by Southern analysis with the 5′ probe. Heterozygous mice were then interbred to obtain homozygous knockout and wild-type control mice. Mice were subsequently genotyped by PCR using primers specific for the wild-type and the targeted allele.

Behavioral Test

We used the rotorod test in this study, which is a test used commonly to score the severity of motor impairment in rodents. Mice were placed on an accelerating rotorod (ENV-575M, Med Associates, Inc., St. Albans, VT) and the time that a mouse stayed on the rotating drum was recorded. Two behavioral patterns noted on loss of balance on the drum were recorded: falling off the rotating rod and clinging to the rotorod with complete "passive" ride around the rod (Paylor et al., 1999). In the latter behavior, the mouse either continued to walk when it reached the top of the rod, or clung around the rod a second time. Behaviors were divided operationally into two categories. For active performing mice, they never passively clung around the rotorod, whereas mice that clung around the rod at least one time during each trial were defined as passive performing mice. For the active mice, the latency to fall was recorded for each trial. For the passive mice, the latency to fall off the rotorod, or the latency to the first cling around (latency to cling) was recorded. Passive performing mice were allowed to continue to walk on the rotorod after the first passive rotation. Thus, the data for latency to fall in the passive mice represented the whole time spent on the rotating rod with several passive rotations. Each mouse underwent three trials per a day with a 45-min intertrial interval and these tests were conducted over 3 successive days. A two-way ANOVA [genotype × trial] with repeated measures was used to analyze the latency to fall or to cling.

Immunohistochemistry for Tyrosine Hydroxylase

Immunolabeling using anti-tyrosine hydroxylase (TH) antibody (TH-16; dilution 1:10,000; Sigma Biosciences, St. Louis, MO) was detected by the avidin-biotinylated horseradish peroxidase complex method (Vectastain ABC elect kit, Burlingame, CA).

Neurochemical Analysis

Contents of dopamine (DA) and its metabolites 3,4-dihydroxy-phenylacetic acid (DOPAC) and homovanillic acid (HVA) were measured by high-performance liquid chromatography (HPLC) equipped with an electrochemical detection system (Kobayashi et al., 1994). Tissues were homogenized in 5 volumes of 0.2 M perchloric acid containing 0.1 M ethylenediaminetetraacetic acid (EDTA) and 100 ng/ml of isoproterenol. After centrifugation of the tissue homogenates, the pH of the supernatants was adjusted to 3.0 by adding 1 M sodium acetate. The samples were injected into the HPLC system with the mobile phase containing 0.1 M sodium citrate,

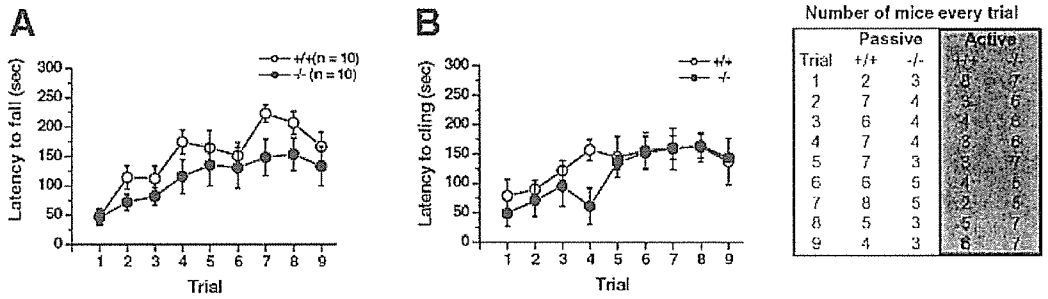

Fig. 2. Results of rotorod motor skill learning test conducted in 12-month-old parkin-deficient and wild-type mice. **A:** Latency to fall. Wild-type (+/+) (n = 10) and knockout (−/−) mice (n = 10) showed equivalent performance and motor learning. The mean ± SEM latency to fall is shown for each trial. **B:** Latency to cling to the rod in passive performing mice. Some mice rode around the rod at least once during training. Number of mice in every trial is tabulated. Active performance, mice that never passively rode around the rotorod (without clinging to the rod); passive performance, mice that rode around the rod at least once during training.

0.1 M citric acid, 0.5 mM sodium octane sulfonate, 0.15 mM EDTA, and 12% methanol (pH 3.5). The detector potential was maintained at 0.75 V vs. the Ag/AgCl electrode.

Ex Vivo Autoradiography

Chemicals. Standard compounds and precursors for labeling of (+)-α-[^{11}C]dihydrotetrabenazine ([^{11}C]DTBZ), [^{11}C]β-CFT (2β-carbomethoxy-3 β-(4-fluorophenyl)tropane: dopamine transporter probe). [^{11}C]SCH23390 (D1 receptor probe) and [^{11}C]raclopride (D_2 receptor probe) were purchased from RBI (Natick, MA). The enzymes for L-[β-^{11}C]DOPA synthesis, alanine racemase (EC 5.1.1.1.), D-amino acid oxidase (EC 1.4.3.3.) and β-tyrosinase (EC 4.1.99.2), were purchased from Ikeda Food Research Co. (Hiroshima, Japan).

Synthesis of [^{11}C]-Labeled Compounds. Carbon-11 (^{11}C) was produced by ^{14}N(p,α)^{11}C nuclear reaction using a cyclotron (HM-18, Sumitomo Heavy Industry, Tokyo) at Hamamatsu Photonics PET center and obtained as [^{11}C]CO_2. [^{11}C]β-CFT and [^{11}C]SCH23390 were labeled with ^{11}C by *N*-methylation of the corresponding nor-compounds with [^{11}C]methyl iodide prepared from [^{11}C]CO_2. [^{11}C]DTBZ and [^{11}C]raclopride were synthesized by *O*-methylation of the corresponding nor-compounds with [^{11}C]methyl iodide. The radiochemical and chemical purities used were >98% and 99%, respectively, and the specific radioactivity ranged from 182–201 GBq/μmol for [^{11}C]DTBZ, 152–181 GBq/μmol for [^{11}C]β-CFT, from 144–162 GBq/μmol for [^{11}C]SCH23390, and from 154–177 GBq/μmol for [^{11}C]raclopride, respectively. L-[β-^{11}C]DOPA (L-3,4-dihydroxyphenylalanine) was synthesized using a combination of organic synthesis and multi-enzymatic procedures using an automated synthesizer. The radiochemical and chemical purities of L-[β-^{11}C]DOPA were >98% and 99%, respectively. After analysis for identification, the solution was passed through a 0.22 μm pore size filter before intravenous (i.v.) administration.

Ex-vivo Imaging. Each labeled compound was injected i.v. at a dose of ca. 1 MBq/g body weight via the tail vein. The animals were sacrificed by decapitation under halothane anesthesia 30 min post-injection for [^{11}C]DTBZ, [^{11}C]SCH23390, and [^{11}C]raclopride, and 60 min post-injection for L-[β-^{11}C]DOPA and [^{11}C]β-CFT. The interval between injection of tracer and sacrifice for each labeled compound was determined based on data from previous reports (Inoue et al., 1991; Tsukada et al., 1994; Takamatsu et al., 2004). The brain was removed immediately, frozen by 2-methyl butane at −20°C, and 2-mm thick brain slices that included the striatal and cerebellar regions were prepared with a brain matrix (RBS-02, Neuroscience Inc., Tokyo, Japan). These slices were contacted with phospho imaging plate for 30 min, and the regional distribution of radioactivity was determined using a phospho imaging plate reader (BAS-1500 MAC, Fuji Film Co., Tokyo, Japan). The radioactivity in the cerebellum was used as the reference because of the low density of DA receptors in this region (Creese et al., 1975). Vesicular monoamine transporter (VMAT) availability, DA reuptake site availability, and DA (D_1 and D_2) receptor binding activities were expressed as follows: "Binding index" = (RIstr − RIcere)/RIcere, where RIstr was the radioactivity of each labeled ligand in the striatal regions and RIcere was the radioactivity in the cerebellum; for the quantification of dopamine synthesis, "Uptake index" was determined as (RIstr − RIcere)/RIcere, where RIstr was the radioactivity of L-[β-^{11}C]DOPA in the striatal regions, and RIcere was the radioactivity in the cerebellum.

Displacement Study of [^{11}C]raclopride With Methamphetamine

To evaluate the dopamine release from pre-synaptic neurons, saline or methamphetamine (MAP) at a dose of 0.3 mg/kg was injected i.v. 30 min before the injection of [^{11}C]raclopride. Brain slice preparation and imaging procedure were carried out as described above.

Statistical Analysis

All data were expressed as mean ± SEM. Differences between groups were examined for statistical significance using the Student's *t*-test. A *P*-value < 0.05 denoted the presence of a statistically significant difference.

RESULTS

Generation of Parkin-Deficient Mice

To investigate the in vivo roles of parkin and shed light on the pathogenic mechanisms of AR-JP, we generated a new line of mice with a targeted disruption of the *parkin* gene. We deleted exon 2 of *parkin* that encodes most of the N-terminal ubiquitin-like domain whose major role is interaction with the 26S proteasome (Sakata et al., 2003). It is noteworthy that several mutations in exon 2 have been reported in patients with AR-JP (Mata et al., 2004). Due to the lack of exon 2, RNA splicing from exons 1–3 is predicted to change the reading frame, which is capable of causing almost complete dysfunction of parkin. We therefore chose the disruption of exon 2 to generate the parkin-null mutant mouse. Deletion of exon 2 was confirmed at the *parkin* genomic locus by Southern analysis (Fig. 1B). Parkin was absent in the knockout brain based on the analysis using anti-parkin antibody (Fig. 1C). Because τ-GFP cDNA was knockin, we also carried out RT-PCR using an GFP-specific primer and confirmed the presence of GFP transcripts in parkin-deficient mice (data not shown). However, the parkin-τ-GFP fusion protein was not clearly detectable by Western and immunohistochemical analyses (data not shown).

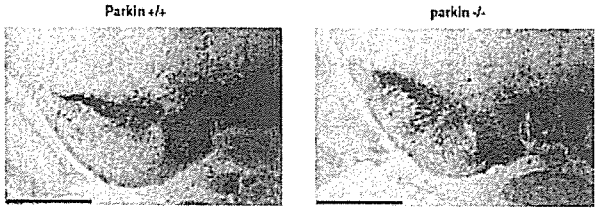

Fig. 3. Immunohistochemical localization of tyrosine hydroxylase (TH) at 3 months in the midbrain and substantia nigra (SN) of parkin-deficient mice and wild-type mice. Normal TH immunoreactivity in the SN. Scale bar = 1 mm.

Phenotype of Parkin$^{-/-}$ Mice

We carried out open field tests of *parkin*$^{-/-}$ mice and observed no significant alterations in their movement behaviors (data not shown). In addition, we eval-

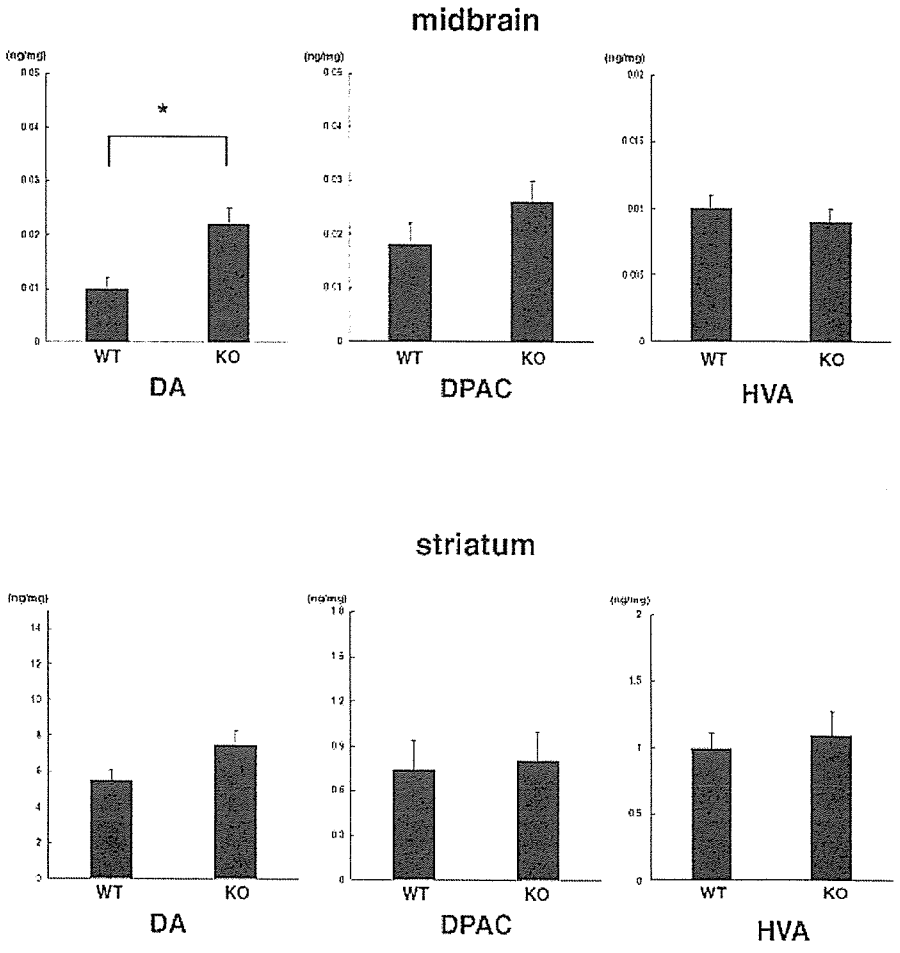

Fig. 4. The levels of DA and its metabolites (DOPAC and HVA) measured at 12 months in the midbrain and striatum in wild-type (WT) (n = 10) and parkin-deficient (KO) mice (n = 10). Concentrations of DA, DOPAC, and HVA were determined by HPLC with electrochemical detection. Data are expressed as mean ± SEM. *P < 0.01.

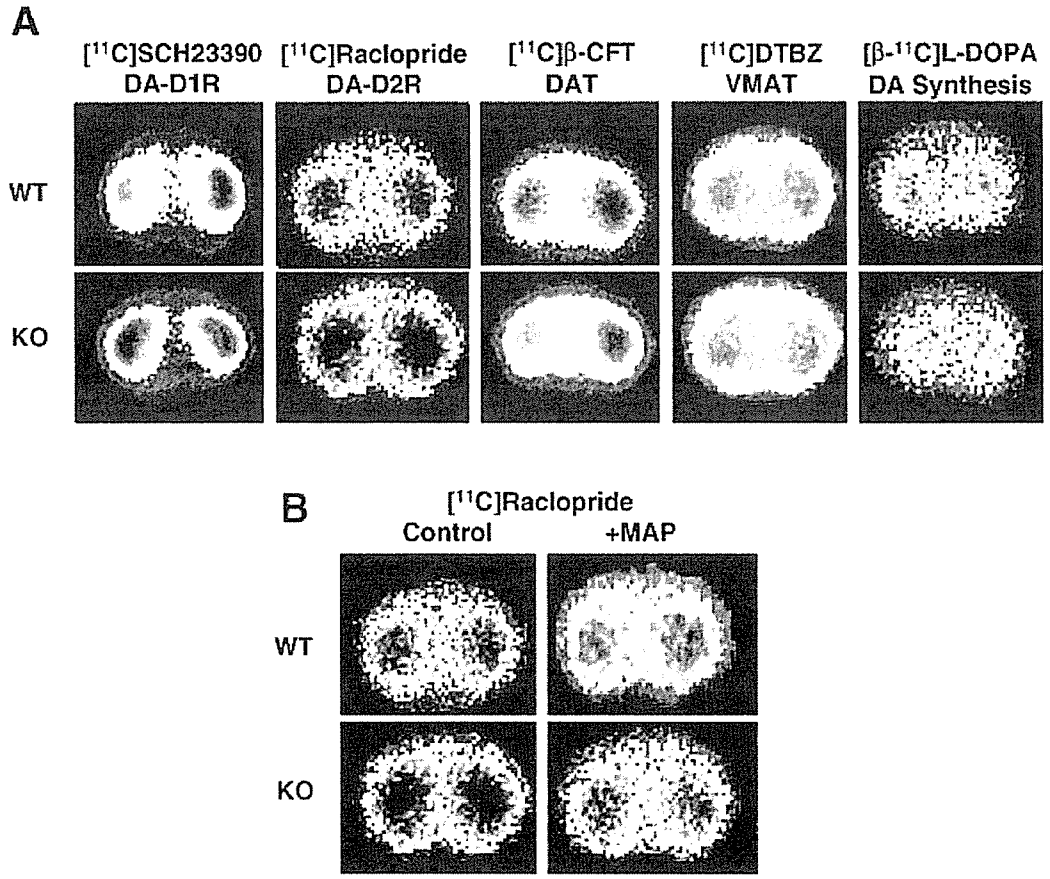

Fig. 5. Autoradiographic images. **A:** Comparison of striatal dopaminergic parameters of DA synthesis, DA receptors (D_1 and D_2), DAT, and VMAT between wild-type (WT) and parkin-deficient (KO) mice. **B:** Effects of methamphetamine (MAP) on striatal [^{11}C]raclopride binding in WT and KO mice. Saline or MAP at a dose of 0.3 mg/kg was injected i.v. 30 min before the injection of [^{11}C]raclopride. Brain slice preparation and imaging procedure were carried out as described in Materials and Methods.

uated these mice at 12 months of age using the rotorod task and found that *parkin*$^{-/-}$ (n = 10) and wild-type mice (n = 10) exhibited similar latencies for remaining on the rotating rod (Fig. 2), confirming the lack of any behavioral deficit. Furthermore, DAergic neurons of parkin-deficient mice were morphologically normal by immunohistochemical analysis with an antibody specific for TH (Fig. 3). Indeed, quantification of the number of DAergic neurons of the mutant and control mice (n = 6 each) at 3 months showed similar numbers of TH-positive neurons in SN and LC (data not shown).

Neurochemical Analysis

Next, we measured the levels of DA and its major metabolites DOPAC and HVA in *parkin*$^{-/-}$ and control mice (n = 10) at 12 months by HPLC with electrochemical detection. In the midbrain including SN, parkin-deficiency was associated with a significant increase in DA level but no change in DOPAC and HVA levels (Fig. 4). In the striatum, no changes in DA, DOPAC, and HVA levels were noted in *parkin*$^{-/-}$ mice compared to the wild-type.

Ex Vivo Autoradiography Study

Figure 5 shows representative autoradiographic images. The levels of two major DA receptors, D_1 and D_2, were measured at 12 months and expressed as the binding index by ex vivo autoradiography using receptor antagonists [^{11}C]SCH23390 and [^{11}C]raclopride, respectively. Quantitative analysis showed that the receptor binding levels of both D_1 and D_2 in the striatum of *parkin*$^{-/-}$ mice (D_1, n =7; D_2, n = 6) were higher than those of normal mice (D_1, n = 5; D_2, n = 6), although the binding index of dopamine transporter (DAT) and vesicular monoamine transporter (VMAT) using [^{11}C]β-CFT and [^{11}C]DTBZ, respectively, were similar (Fig. 6A)

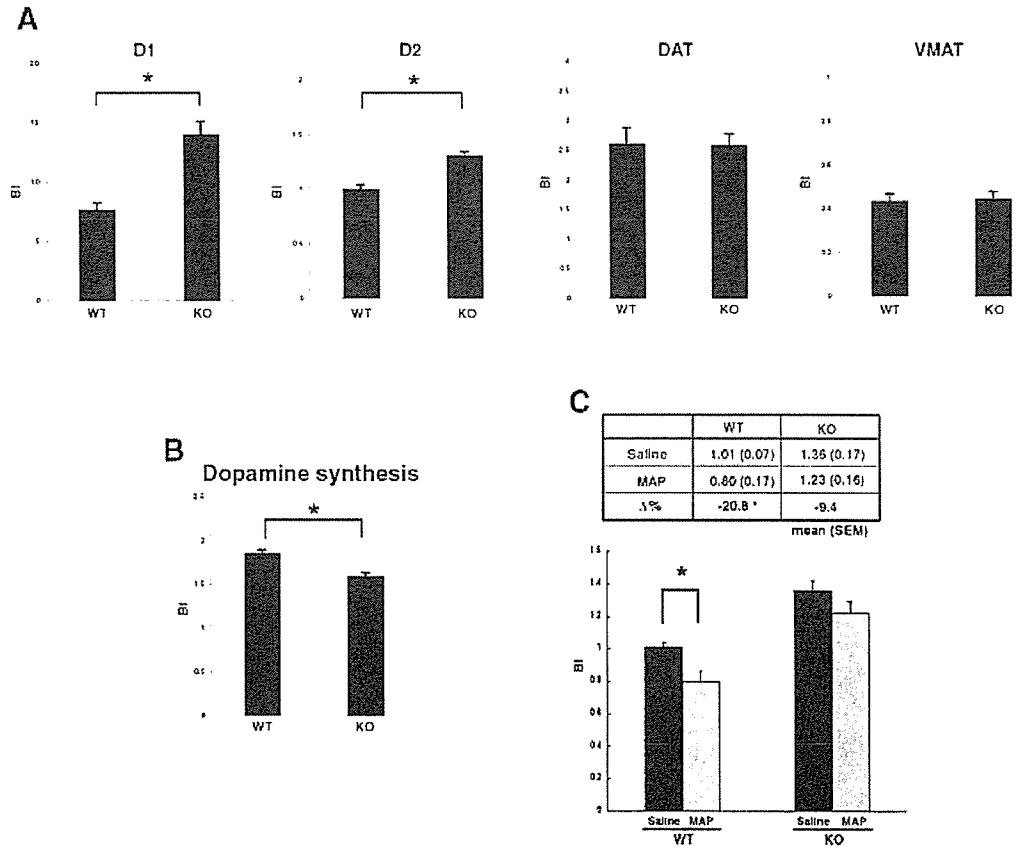

Fig. 6. Quantitative analysis of ex vivo autoradiography. **A:** Binding index for DA receptors (D_1 and D_2), DAT, and VMAT in the striatum of mice aged 12 months. **B:** DA synthesis in the striatum of mice aged 12 months. **C:** DA release of mice aged 12 months. Values of striatal [^{11}C]raclopride binding after administration of methamphetamine (MAP) or saline in wild-type and parkin-null mice are tabulated. %Δ, percentage difference [(methamphetamine binding index − saline binding index)/saline binding index] × 100. Data are expressed as mean ± SEM. $*P < 0.01$.

in *parkin*$^{-/-}$ mice (DAT, n = 7; VMAT, n = 6) and normal mice (DAT, n = 5; VMAT, n = 6). Furthermore, DA synthesis determined by conversion of L-[β-^{11}C]DOPA to [β-^{11}C]DA was significantly decreased in *parkin*$^{-/-}$ mice (n = 8) compared to control mice (n = 8) (Fig. 6B).

Finally, we analyzed DA release in the striatum of *parkin*$^{-/-}$ mice using dopamine D_2 receptor antagonist [^{11}C]raclopride after treatment of methamphetamine (MAP) or saline. [^{11}C]Raclopride is considered to compete with endogenous DA at D_2 receptor sites, and competition between [^{11}C]raclopride and endogenous DA has been used recently to measure the level of DA release (Tsukada et al., 2000; Piccini et al., 2003). The binding of [^{11}C]raclopride was decreased in the presence of high levels of released endogenous DA in the synaptic clefts. The release capacity of DA can be estimated by a decrease in the binding level after methamphetamine-induced release of endogenous DA. Ex vivo autoradiography conducted at 12 months using [^{11}C]raclopride showed that the activity of DA release in *parkin*$^{-/-}$ mice (n = 8) was clearly reduced relative to that in wild-type mice (n = 9) (Fig. 6C).

DISCUSSION

Several studies have reported deletion of the mouse *parkin* gene but against expectation, the majority of such mice exhibited subtle phenotypes without causing massive loss of DAergic neurons (Goldberg et al., 2003; Itier et al., 2003; Von Coelln et al., 2004; Perez and Palmiter, 2005). Our parkin-null mice showed no obvious behavioral deficit; testing mouse mobility by using the open field test (data not shown) and rotorod test (Fig. 2) showed no reduction in locomotor activity. Histologically, no change in TH-positive nigra neurons was noted in parkin-deficient mice (Fig. 3), and no significant decrease in DAT was observed (Fig. 6A). [^{11}C]β-CFT shows a high affinity to DAT and accurately reflects a terminal density close to that of DA neurons, which could be potentially useful in tracing the drop out of DA neurons over time. These results show clearly the lack of any neurodegeneration in the cell bodies of DA neurons and nerve terminals of parkin deficient mice.

In an attempt to determine the pathologic state of parkin-deficient mice, we assessed the binding of D_1 and D_2 receptors by ex vivo autoradiography. We used the [^{11}C]SCH23390 and [^{11}C]raclopride ligands against the D_1 and D_2 receptors, respectively. Intriguingly, parkin deficiency was associated with marked elevation of both D_1 and D_2 receptors. Indeed, previous studies reported that although striatal D_2 binding increased in untreated patients with PD, adaptive postsynaptic mechanisms and treatment decreased this as the condition advanced (Ahlskog et al., 1991; Brooks et al., 1992; Ichise et al., 1999). In a study of AR-JP patients, Scherfler et al. (2004) reported a global decrease in D_2 receptor and argued for parkin genetic defect itself or susceptibility to receptor downregulation after long-term exposure to dopaminergic agents. Taking into account the results of the present study, we consider the latter scenario; i.e., long-term exposure to dopaminergic agents, to result in downregulation of D_2 receptor. The decrease in DA concentration in synaptic clefts in early-stage PD is expected to lead to increased expression of D_2. Goldberg et al. (2003) reported that DA actually increases extracellularly in knockout mice.

We next measured DA release in knockout mice. When endogenous DA binds to the D_2 receptor, it competes with the antagonist [^{11}C]raclopride. This process allows synaptic DA levels to be estimated indirectly from changes in D_2 receptor binding. Elevation of DA synaptic concentrations can be achieved in vivo by administration of DA releaser such as amphetamine. The level of binding index in parkin-deficient mice was significantly higher than that of control mice, indicating a low DA release capacity in knockout mice (Fig. 6C). A similar method showed a decrease in release capacity of DA in PD (Piccini et al., 2003). However, this level of alteration of DA release potential is not sufficient to cause atrophy and degeneration of DAergic neurons, thus explaining the lack of a clear phenotype in knockout mice. Indeed, the open field and rotorod tests showed no reduction in locomotor activity, as mentioned above.

Quantitative analysis showed no differences in dopamine levels in the striatum of mutant and wild-type mice, although higher DA concentrations were noted in the midbrain of knockout mice relative to the control. This regional difference may be due to either accumulation of DA consequent to the low level of DA release, or due to increased DA reuptake. Although the expression levels of DAT and VMAT were not different between the two types of mice, further research is necessary to determine their precise functions. It is well-known that [^{18}F]DOPA undergoes reuptake in DAergic neurons and metabolizes to [^{18}F]DA, which is indicative of the synthetic capacity of DA involved in PD (Dagher, 2001; de la Fuente-Fernandez and Stoessl, 2002). Likewise, L-[β-^{11}C]DOPA is also metabolized to form [β-^{11}C]DA. Using this method, the overall synthetic capacity of DA was significantly low in knockout mice compared to wild-type mice (Fig. 6B). Excess DA in neurons may induce down-regulation of this synthetic capacity. In this regard, abnormal reuptake of [^{18}F]DOPA was reported previously in AR-JP patients (Broussolle et al., 2000; Hilker et al., 2001; Portman et al., 2001; Khan et al., 2002; Thobois et al., 2003; Scherfler et al., 2004). In contrast, the levels of DOPAC and HVA in the ventral midbrain were apparently normal in our knockout mice. This finding may be dependent on the regulation of activities of various enzymes that metabolize catecholamines, which compensate the altered DA transmission in parkin deficiency.

In conclusion, we have shown in the present study the presence of low levels of DA release in parkin-deficient mice, suggesting that DAergic neurons could behave abnormally before neuronal death.

REFERENCES

Ahlskog JE, Richelson E, Nelson A, Kelly PJ, Okazaki H, Tyce GM, van Heerden JA, Stoddard SL, Carmichael SW. 1991. Reduced D2 dopamine and muscarinic cholinergic receptor densities in caudate specimens from fluctuating parkinsonian patients. Ann Neurol 30:185–191.

Brooks DJ, Ibanez V, Sawle GV, Playford ED, Quinn N, Mathias CJ, Lees AJ, Marsden CD, Bannister R, Frackowiak RS. 1992. Striatal D2 receptor status in patients with Parkinson's disease, striatonigral degeneration, and progressive supranuclear palsy, measured with ^{11}C-raclopride and positron emission tomography. Ann Neurol 31:184–192.

Broussolle E, Lucking CB, Ginovart N, Pollak P, Remy P, Durr A. 2000. [^{18}F]-dopa PET study in patients with juvenile-onset PD and parkin gene mutations. Neurology 55:877–879.

Chung KK, Zhang Y, Lim KL, Tanaka Y, Huang H, Gao J, Ross CA, Dawson VL, Dawson TM. 2001. Parkin ubquitinates the alpha-synuclein-interacting protein, synphilin-1: implications for Lewy-body formation in Parkinson disease. Nat Med 7:1144–1150.

Creese I, Burt DR, Snyder SH. 1975. Dopamine receptor binding: differentiation of agonist and antagonist states with [^{3}H]dopamine and [^{3}H]haloperidol. Life Sci 17:993–1002.

Dagher A. 2001. Functional imaging in Parkinson's disease. Semin Neurol 21:23–32.

de la Fuente-Fernandez R, Stoessl AJ. 2002. Parkinson's disease: imaging update. Curr Opin Neurol 15:477–482.

Fukuda T. 1994. 2-methyl-1,2,3,4-tetrahydroisoquinoline does dependently reduce the number of tyrosine hydroxylase-immunoreactive cells in the substantia nigra and locus ceruleus of C57BL/6J mice. Brain Res 639:325–328.

Goldberg MS, Fleming SM, Palacino JJ, Cepeda C, Lam HA, Bhatnagar A, Meloni EG, Wu N, Ackerson LC, Klapstein GJ, Gajendiran M, Roth BL, Chesselet MF, Maidment NT, Levine MS, Shen J. 2003. Parkin-deficient mice exhibit nigrostriatal deficits but not loss of dopaminergic neurons. J Biol Chem 278:43628–43635.

Hilker R, Klein C, Ghaemi M, Kis B, Strotmann T, Ozelius LJ, Lenz O, Vieregge P, Herholz K, Heiss WD, Pramstaller PP. 2001. Positron emission tomographic analysis of the nigrostriatal dopaminergic system in familial parkinsonism associated with mutations in the parkin gene. Ann Neurol 49:367–376.

Ichise M, Kim YJ, Ballinger JR, Vines D, Erami SS, Tanaka F, Lang AE. 1999. SPECT imaging of pre- and postsynaptic dopaminergic alterations in L-dopa-untreated PD. Neurology 52:1206–1214.

Imai Y, Soda M, Inoue H, Hattori N, Mizuno Y, Takahashi R. 2001. An unfolded putative transmembrane polypeptide, which can lead to endoplasmic reticulum stress, is a substrate of Parkin. Cell 105:891–902.

Inoue O, Kobayashi K, Tsukada H, Itoh T, Långström B. 1991. Difference in in vivo receptor binding between ^{3}H-N-methylspiperone and ^{3}H-raclopride. J Neural Transm 85:1–10.

Itier JM, Ibanez P, Mena MA, Abbas N, Cohen-Salmon C, Bohme GA, Laville M, Pratt J, Corti O, Pradier L, Ret G, Joubert C, Periquet M, Araujo F, Negroni J, Casarejos MJ, Canals S, Solano R, Serrano A, Gallego E, Sanchez M, Denefle P, Benavides J, Tremp G, Rooney TA, Brice A, Garcia de Yebenes J. 2003. Parkin gene inactivation alters behavior and dopamine neurotransmission in the mouse. Hum Mol Genet 12:2277–2291.

Khan NL, Brooks DJ, Pavese N, Sweeney MG, Wood NW, Lees AJ, Piccini P. 2002. Progression of nigrostriatal dysfunction in a parkin kindred: an [^{18}F]dopa PET and clinical study. Brain 125:2248–2256.

Kitada T, Asakawa S, Hattori N, Matsumine H, Yamamura Y, Minoshima S, Yokochi M, Mizuno Y, Shimizu N. 1998. Mutations in the parkin gene cause autosomal recessive juvenile parkinsonism. Nature 392:605–608.

Kobayashi K, Morita S, Mizuguchi T, Sawada H, Yamada K, Nagatsu I, Fujita K, Nagatsu T. 1994. Functional and high level expression of human dopamine beta-hydroxylase in transgenic mice. J Biol Chem 269:29725–29731.

Mata IF, Lockhart PJ, Farrer MJ. 2004. Parkin genetics: one model for Parkinson's disease. Hum Mol Genet 13:R127–133.

Paylor R, Hirotsune S, Gambello MJ, Yuva-Payor L, Crawley JN, Wynshaw-Boris A. 1999. Impaired learning and motor behavior in heterozygous Pafah1b1 (Lis 1) mutant mice. Learn Mem 6:521–537.

Perez FA, Palmiter RD. 2005. Parkin-deficient mice are not a robust model of parkinsonism. Proc Natl Acad Sci U S A 102:2174–2179.

Periquet M, Corti O, Jacquier S, Brice A. 2005. Proteomic analysis of parkin knockout mice: alterations in energy metabolism, protein handling and synaptic function. J Neurochem 95:1259–1276.

Piccini P, Pavese N, Brooks DJ. 2003. Endogenous dopamine release after pharmacological challenges in Parkinson's disease. Ann Neurol 53:647–653.

Portman AT, Giladi N, Leenders KL, Maguire P, Veenma-van der Duin L, Swart J, Pruim J, Simon ES, Hassin-Baer S, Korczyn AD. 2001. The nigrostriatal dopaminergic system in familial early onset parkinsonism with parkin mutations. Neurology 56:1759–1762.

Sakata E, Yamaguchi Y, Kurimoto E, Kikuchi J, Yokoyama S, Yamada S, Kawahara H, Yokosawa H, Hattori N, Mizuno Y, Tanaka K, Kato K. 2003. Parkin binds the Rpn10 subunit of 26S proteasomes through its ubiquitin-like domain. EMBO Rep Mar; 4:301–306.

Scherfler C, Khan NL, Pavese N, Eunson L, Graham E, Lees AJ, Quinn NP, Wood NW, Brooks DJ, Piccini PP. 2004. Striatal and cortical pre- and postsynaptic dopaminergic dysfunction in sporadic parkin-linked parkinsonism. Brain 127:1332–1342.

Shimura H, Hattori N, Kubo S, Mizuno Y, Asakawa S, Minoshima S, Shimizu N, Iwai K, Chiba T, Tanaka K, Suzuki T. 2000. Familial Parkinson disease gene product, parkin, is a ubiquitin-protein ligase. Nat Genet 25:302–305.

Takamatsu H, Kakiuchi T, Noda A, Uchida H, Nishiyama S, Ichise R, Iwashita A, Mihara K, Yamazaki S, Matsuoka N, Tsukada H, Nishimura S. 2004. An application of a new planar positron imaging system (PPIS) in a small animal: MPTP-induced parkinsonism in mouse. Ann Nucl Med 18:427–431.

Thobois S, Ribeiro MJ, Lohmann E, Durr A, Pollak P, Rascol O, Guillouet S, Chapoy E, Costes N, Agid Y, Remy P, Brice A, Broussolle E. 2003. Young-onset Parkinson disease with and without parkin gene mutations: a fluorodopa F 18 positron emission tomography study. Arch Neurol 60:713–718.

Tsukada H, Harada N, Nishiyama S, Ohba H, Kakiuchi T. 2000. Cholinergic neuronal modulation alters dopamine D2 receptor availability in vivo by regulating receptor affinity induced by facilitated synaptic dopamine turnover: positron emission tomography studies with microdialysis in the conscious monkey brain. J Neurosci 20:7067–7073.

Tsukada H, Lindner KJ, Hartvig P, Tani Y, Bjurling P, Kihlberg T, Westerberg G, Watanabe Y, Långström B. 1994. Effect of 6R-L-erythro-5, 6,7,8-tetrahydrobiopterin on in vivo L-[β-^{11}C] DOPA turnover in the rat striatum with infusion of L-tyrosine. J Neural Transm 95:1–15.

Von Coelln R, Thomas B, Savitt JM, Lim KL, Sasaki M, Hess EJ, Dawson VL, Dawson TM. 2004. Loss of locus coeruleus neurons and reduced startle in parkin null mice. Proc Natl Acad Sci U S A 101: 10744–10749.

Artificial Organs
31(2):148–170, Blackwell Publishing, Inc.

Thoughts and Progress

Extracorporeal Bioartificial Liver Using the Radial-flow Bioreactor in Treatment of Fatal Experimental Hepatic Encephalopathy

*Hideki Kanai, *¶Hideki Marushima, †Naofumi Kimura, ‡Takamasa Iwaki, §Masaya Saito, ¶Haruka Maehashi, ¶Keiko Shimizu, ¶Makiko Muto, ¶Takahiro Masaki, ¶Kiyoshi Ohkawa, §Keitaro Yokoyama, §Masaaki Nakayama, **Tohru Harada, **Hiroshi Hano, ††Yoshiaki Hataba, ‡‡Takahiro Fukuda, ¶¶Masahiko Nakamura, ¶¶Naoto Totsuka, ¶¶Shutaro Ishikawa, *Yasuki Unemura, *Yuji Ishii, *Katsuhiko Yanaga, and §§Tomokazu Matsuura

*Department of Surgery, †Department of Pharmacology II, ‡Laboratory Animal Facilities, §Department of Internal Medicine, ¶Department of Biochemistry I, **Department of Pathology, ††Institute of DNA Medicine, ‡‡Department of Neuroscience, §§Department of Laboratory Medicine, The Jikei University School of Medicine, Tokyo, and ¶¶Biott Co. Ltd., Tokyo, Japan

Abstract: An extracorporeal bioartificial liver (BAL) that could prevent death from hepatic encephalopathy in acute hepatic insufficiency was aimed to develop. A functional human hepatocellular carcinoma cell line (FLC-4) was cultured in a radial-flow bioreactor. The function of the BAL was tested in mini-pigs with acute hepatic failure induced by α-amanitin and lipopolysaccharide. When the BAL system was connected with cultured FLC-4 to three pigs with hepatic dysfunction, all demonstrated electroencephalographic improvement and survived. Relatively low plasma concentrations of S-100 β protein, as a marker of astrocytic damage, from pigs with hepatic failure during BAL therapy were noted. BAL therapy can prevent irreversible brain damage from hepatic encephalopathy in experimental acute hepatic failure. **Key Words:** Acute hepatic failure—Radial-flow bioreactor—Cerebral edema—Astrocytes—α-Amanitin.

doi:10.1111/j.1525-1594.2007.00354.x

Received September 2005; revised July 2006.

Address correspondence and reprint requests to Dr. Tomokazu Matsuura, Department of Laboratory Medicine, The Jikei University School of Medicine, 3-25-8 Nishi-shinbashi, Minato-ku, Tokyo 105-8461, Japan. E-mail: matsuurat@jikei.ac.jp

A clinically effective bioartificial liver (BAL) requires development of a high-density cell culture module and a highly functioning liver cell line. We sought to develop a high-performance BAL to avoid lethal hepatic encephalopathy in acute hepatic insufficiency and establish the BAL as an extracorporeal circulation therapy able to surpass conventional blood purification procedures. Our extracorporeal BAL support system used a highly functional human hepatocellular carcinoma (HCC) cell line (FLC-4) cultured in a radial-flow bioreactor (RFB) (1,2). The RFB is packed with cell-adhesion scaffolds in a cylindrical array (Fig. 1A,B). The culture medium or the plasma flows from the periphery of the cylindrical module to the center. One important problem when cells are cultured densely is delivery of sufficient oxygen and nutrients even when these are plentiful at the inflow site. As a result, we could culture cells successfully at a density of 10^8/mL.

We have currently tested the BAL in mini-pigs with acute hepatic failure induced by α-amanitin, a mushroom-derived poison, and lipopolysaccharide (LPS), while monitoring with electroencephalography (EEG) to assess the effectiveness of BAL against hepatic encephalopathy. We measured the plasma levels of S-100 β protein, a marker of damage to astrocytes (3).

MATERIALS AND METHODS

Mini-pigs and monitoring

Male mini-pigs (CSK-MS) weighing 10–15 kg were a generous gift from Chugai Pharmaceutical (Tokyo, Japan). Prior to the experiments, they were maintained for 1–4 weeks at the Laboratory Animal Facilities of the Jikei University School of Medicine, receiving standard chow and water ad libitum. The study was approved by the institution's committee concerning animal experimentation.

Acute hepatic failure model

During inhalation anesthesia with 3–4% isoflurane, 0.05 mg/kg of α-amanitin (Calbiochem, Darmstadt, Germany) and 1 μg/kg of LPS (Sigma, St. Louis, MO, USA) dissolved in 10 mL of saline was administered via the splenic vein. Fifty percent

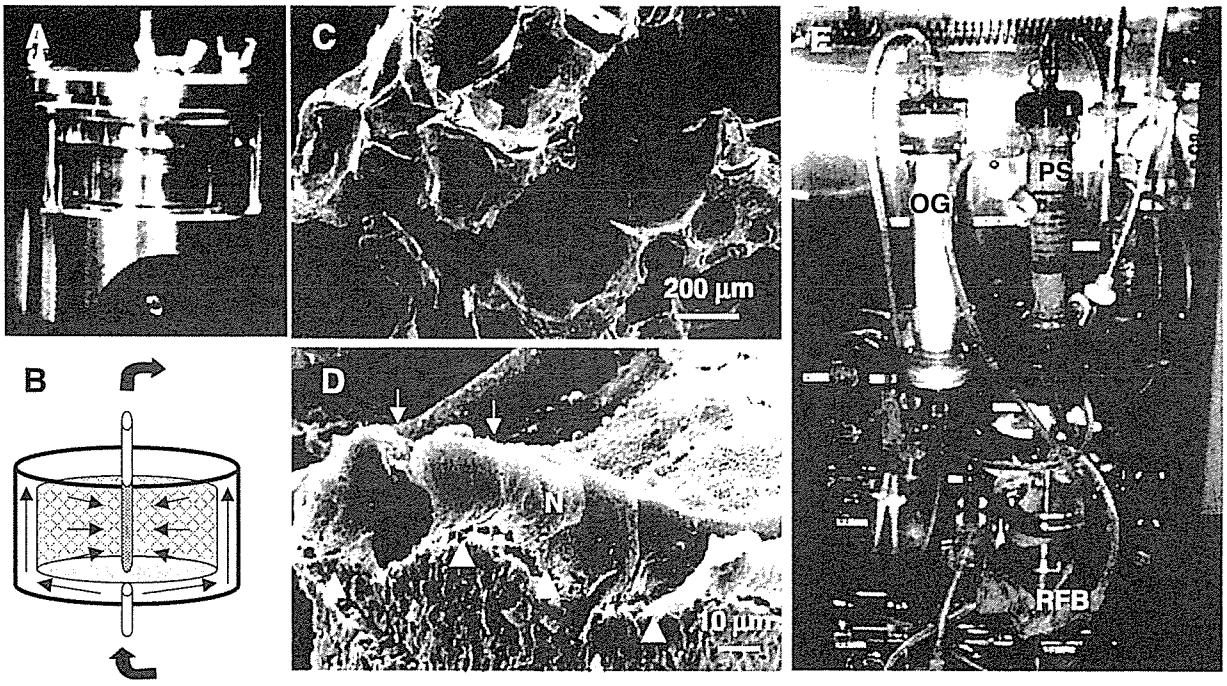

FIG. 1. (A,B) The RFB. The RFB is packed with cell-adhesion scaffolds in a cylindrical array. Culture medium or plasma flows from the periphery of the cylindrical module to the center. (C,D) Scanning electron microscopic (SEM) observations in FLC-4 cells cultured on hydroxyapatite beads in the RFB. FLC-4 cells form a single layer on porous hydroxyapatite beads in a cubic array. The arrow heads indicate the basal side of cells, while the arrows show the apical side of cells. N, nucleus. (E) The extracorporeal BAL system. From blood obtained from an artery, and plasma is separated from cells at 10–15 mL/min by the plasma separator (PS) and flows into the BAL after taking up oxygen from the oxygeneter (OG). The entire device is maintained consistently at 37°C. The purified plasma is mixed with blood cells and returned to a vein.

glucose solution and 7% sodium bicarbonate were injected as required during the monitoring of venous blood glucose and arterial blood acid-base parameters.

BAL using the RFB

The RFB (Biott, Tokyo, Japan) is a cell-filling type bioreactor of 15-mL capacity in which a cylindrical module is filled up with porous hydroxyapatite beads (PENTAX, Tokyo, Japan) with a diameter of approximately 1 mm (1) (Fig. 1A,B,C). The culture system consists of the RFB, a reservoir-adjusting culture fluid, a circulation pump, and an automatic controller to adjust the dissolved oxygen content and the pH of the culture fluid. We injected 10^8 of FLC-4 cells, a human HCC cell line, into the reservoir, which contained ASF 104 culture medium (Ajinomoto, Tokyo, Japan) with 2% fetal bovine serum (FBS) and set the circulated pump at 10 mL/min for seeding and attaching cells into the porous hydroxyapatite beads in the RFB (Fig. 1D). The circulation culture at 25 mL/min was continued for 10 days after adhesion of the cells was confirmed and FLC-4 cells grew 10^9 in the RFB. We used the RFB almost completely filled with cells as the BAL.

Extracorporeal circulation using the RFB

Arterial blood was extracted at 20–30 mL/min, and plasma was separated at 10–15 mL/min by a plasma separator (Plasmaflo, OP-02W, Asahi Kasei Medical, Tokyo, Japan) and allowed to circulate through the BAL after passage through an oxygenator (silicone rubber tube module M40-3000, Nagayanagi, Tokyo, Japan) (Fig. 1E). The entire device was maintained constantly at 37°C. Together with the separated blood cells, the purified plasma was returned to the animal via the cervical vein. The extracorporeal circulation time in this experiment was 4–6 h. Intravenous treatment with 50% glucose and 7% sodium bicarbonate solution continued after the BAL extracorporeal circulation. Heparin was injected as an anticoagulant. At initiation of extracorporeal circulation, an intra-

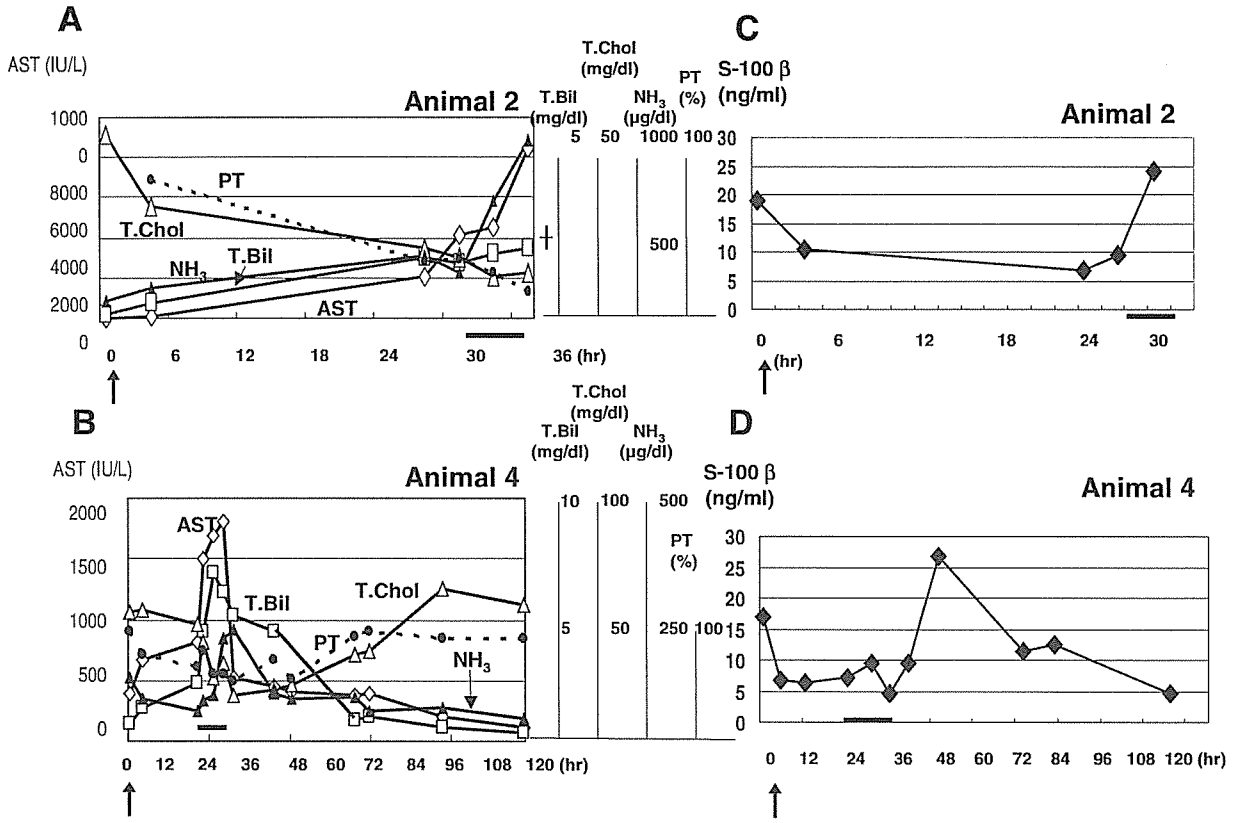

FIG. 2. (A) Time course of biochemical data in control (animal 2) developing hepatic failure after administration of α-amanitin and LPS. Plasma was perfused through the RFB without FLC-4 cells. Neither control animal (animals 1 and 2) recovered at any time from fatal hepatic failure. (B) Time course of biochemical data in an animal (animal 4) developing acute hepatic failure after administration of α-amanitin and LPS. Plasma was perfused through the RFB containing FLC-4 cells beginning 12 h or more after toxin administration. All three animals (animals 4, 5, and 6) treated by BAL therapy survived. The arrow indicates the time of α-amanitin and LPS administration. Black bar indicates extracorporeal BAL perfusion. AST, aspartate amino transferase; T.Bil, total bililbin; T.Chol, total cholesterol; PT, prothrombin time. (C) S-100 β protein in plasma from an animal with untreated acute hepatic failure, showing a marked increase that suggested severe astrocytic damage. (D) This increase is less prominent during BAL extracorporeal circulation.

venous injection of 1000 units was given. Heparin then was infused into the withdrawn arterial blood at 500 units/h.

Enzyme-linked immunosorbent assay (ELISA) for S-100 β in plasma

We measured S-100 β protein in plasma as a systemic marker of damage to brain astrocytes in pigs with acute hepatic failure using an ELISA kit (Yanaihara Institute, Shizuoka, Japan).

RESULTS AND DISCUSSION

In the present preclinical study, our ultimate aim was to find a way to prevent or reverse potentially lethal hepatic encephalopathy in acute hepatic failure using BAL as a bridge to either recovery or transplantation. We used an acute hepatic failure model involving a relatively large animal to test the effectiveness of densely cultured FLC-4 cells in a module for extracorporeal circulation. Devising an acute hepatic failure model in a relatively large animal is extremely difficult. We used the method of Takada et al., who induced acute hepatic failure by injecting α-amanitin and LPS via the portal vein (4). We first established extracorporeal circulation through a BAL system without FLC-4 cells in two animals (animals 1 and 2) with α-amanitin/LPS-induced hepatic dysfunction. The animals died respectively 2 h after initiation of extracorporeal circulation and at a completion point of extracorporeal circulation at 6 h (Fig. 2A). We thus used the BAL system with FLC-4 cells to treat hepatic dysfunction

in three animals (animals 3, 4, and 5), obtaining EEG improvement and survival in all. Figure 2B shows the course of one animal treated by BAL therapy. Even when transaminase and ammonia concentrations in blood were not markedly elevated, many animals that had been injected with α-amanitin and LPS died of hemorrhagic necrosis of the liver with marked cerebral edema. Among the blood tests, the best index of hepatic failure was a decrease in the cholesterol concentration. We therefore administered BAL for 4–6 h, when the EEG showed slowing and plasma cholesterol decreased, about 12–20 h after toxin administration. The three animals with acute hepatic failure showed considerable normalization of slow-wave activity in the EEG after extracorporeal circulation therapy using FLC-4 cultured in the RFB, with ultimate survival.

The reason for the survival of animals with acute hepatic failure treated with the BAL is thought to be the prevention of rapidly progressive cerebral edema. In plasma from a pig dying from hepatic failure, and a surviving animal just after BAL therapy, we measured the plasma levels of S-100 β protein as a marker of hepatic encephalopathy specifically astrocytic damage (3). S-100 β protein had significantly increased in plasma from animals with acute hepatic failure, especially those that died (Fig. 2C). In contrast, we observed that the release of S-100 β protein in plasma was inhibited during BAL therapy and the animal survived (Fig. 2D). This suggested that BAL therapy tended to ameliorate encephalopathy in acute hepatic failure.

Agents potentially responsible for hepatic coma include not only ammonia and manganese compounds, but also an assumed unknown substance with a molecular weight of 5–20 kD (5). Astrocytes form the blood brain barrier (BBB), and sustain nerve cells as they function (6). Increases of the postulated hepatic coma agent in blood induce early functional impairment in astrocytes. However, removal of the unidentified hepatic coma agent(s) is difficult using conventional blood-purifying treatments. We therefore feel an urgent need to develop modalities such as the BAL, in which human liver cells (highly functioning HCC cell lines) are cultured at high density in an RFB. The results of this experiment suggest that BAL can ameliorate hepatic encephalopathy by removal of suspected and/or unknown hepatic coma agents.

CONCLUSIONS

We constructed a compact and high functional BAL system using the RFB and a human HCC cell line FLC-4. Large animals with acute hepatic failure induced by α-amanitin and LPS were able to recover from fatal hepatic encephalopathy, and the result was improved by the extracorporeal circulation therapy using this system.

Acknowledgments: We thank Mr. H. Saito at the Jikei University School of Medicine for SEM technical support, and the technicians of the Division of Central Clinical Laboratory at Jikei University Hospital for blood and biochemical analysis. We also thank the 21 medical students of the Jikei University School of Medicine for their involvement in carrying this study as part of our practice-of-research program between 2001 and 2004.

This study was supported in part by Grants-in-Aids from the University Start-Ups Creation Support System, The Promotion and Mutual Aid Corporation for Private Schools of Japan, and The Japan Health Sciences Foundation (Research on Health Sciences for Drug Innovation, KH71068).

REFERENCES

1. Iwahori T, Matsuura T, Maehashi H, et al. Cyp3a4 inducible model for in vitro analysis of human drug metabolism using a bioartificial liver. *Hepatology* 2003;37:665–73.
2. Saito M, Matsuura T, Masaki T, et al. Reconstruction of liver organoid using a bioreactor. *World J Gastroenterol* 2006;12: 1881–8.
3. Hovsepyan MR, Haas MJ, Boyajyan AS, et al. Astrocytic and neuronal biochemical markers in the sera of subjects with diabetes mellitus. *Neurosci Lett* 2004;21:224–7.
4. Takada Y, Ishiguro S, Fukunaga K, et al. Increased intracranial pressure in a porcine model of fulminant hepatic failure using amatoxin and endotoxin. *J Hepatol* 2001;34:825–31.
5. Yamazaki Z, Fujimori Y, Sanjo K, et al. New artificial liver support system (plasma perfusion detoxification) for hepatic coma. 1978. *Ther Apher* 2000;4:23–5.
6. Matsushita M, Yamamoto T, Gemba H. The role of astrocytes in the development of hepatic encephalopathy. *Neurosci Res* 1999;34:271–80.

Japanese Journal of Applied Physics
Vol. 45, No. 5B, 2006, pp. 4736–4739

Verification of Ultrasonic Thrombolysis Effect by *in Vitro* Experiments

Makoto OGIHARA, Jun KUBOTA, Takashi AZUMA[1], Kazumi ANDO[2], Yasumasa TANIHUJI[2], Shin-ichiro UMEMURA[3] and Hiroshi FURUHATA[4]

Research and Development Center, Hitachi Medical Corporation, Kashiwa, Chiba 277-0804, Japan
[1]*Central Research Laboratory, Hitachi, Ltd., Kokubunji, Tokyo 185-8601, Japan*
[2]*Department of Anesthesiology, Jikei Medical School of Medicine, Tokyo 105-8461, Japan*
[3]*Health Sciences Faculty of Medicine, Kyoto University, Kyoto 606-8507, Japan*
[4]*Medical Engineering Laboratory, Jikei University School of Medicine, Tokyo 105-8461, Japan*

(Received November 30, 2005; accepted February 2, 2006; published online May 25, 2006)

The tissue plasminogen activator (t-PA) has been approved as a thrombolytic agent for treating cerebral thrombosis. It is reported that recanalization occurs earlier in a hyperacute ischemic stroke when both t-PA and transcranial ultrasonication are applied than when t-PA alone is applied. We have developed a therapy-and-diagnostics (T/D) compound transcranial ultrasonic thrombolytic system. To minimize adverse mechanical and thermal biological effects, the frequency of the therapeutic ultrasound (US) beam is selected to be 500 kHz. The diagnostic US beam at 2 MHz is used for monitoring the recanalization. We confirmed the effect of this system using two types of experiment. One determined the recanalization rate and dissolution time of the simulated thrombotic vascular occlusion at narrowed vessels and the other determined the weight decrease of the clot, and both involved exposure to t-PA solution with and without ultrasonication. As a result, the recanalization rate is higher in the US + t-PA (92.3%) than in the t-PA-only (64.1%). The decrease rate is also higher in the US + t-PA (25.4%) than in the t-PA-only (15.1%). [DOI: 10.1143/JJAP.45.4736]

KEYWORDS: medical, diagnostic, therapy, stroke, acute, thrombolysis, clot, t-PA, *in vitro*

1. Introduction

Cerebrovascular accident (CVA) is a condition with the third highest mortality next to cancer and heart disease in Japan. In particular, strokes account for roughly 70% of CVAs. Even if death does not occur, a longer cerebral ischemic interval resulting from CVA often causes paralysis and produces injurious effects. Therefore, it is important to induce clot lysis at the early stage of ischemia. The tissue plasminogen activator (t-PA) has been approved in the EU, the U.S.A., and Japan to be used for the treatment of hyperacute ischemic stroke. It is known that ultrasonication enhances the thrombolysis effect of t-PA.[1–9]

CLOTBUST studies[4,6] show that even the continuous use of 2 MHz normal transcranial Doppler ultrasonography (TCD) accelerates thrombolysis in clinical experiments. The ultrasound (US) spatial peak temporal average intensity (I_{SPTA}) used in this study was about 0.4 W/cm^2.

We know that a lower frequency gets a higher rate of recanalization *in vivo*.[5] If we use low-frequency ultrasound only, we sacrifice the performance of the diagnostic image. Therefore, we use a different type of ultrasound for the therapy beam (T-beam) from that for the diagnostic beam (D-beam). We have developed a T/D compound system that uses ultrasound of 500 kHz and below 0.72 W/cm^2 for the therapy, and that of 2 MHz and below 0.72 W/cm^2 for diagnostics. In this study, we confirmed the effectiveness of this system for *in vitro* experiments.

2. Experimental

2.1 *Ultrasound exposure system*

The developed system is composed of an ultrasound diagnostic unit, a T-beam generator, a T/D compound sector probe and a T/D switching controller (control unit), as shown in Fig. 1. The T/D compound probe irradiates a 500-kHz-frequency ultrasound beam as a T-beam, and a 2-MHz-frequency ultrasound beam as a D-beam. To avoid the risk of intracranial hemorrhage, the direction of the T-beam is targeted at an area around the embolized artery. Ultrasound bioeffects are affected mainly by thermal index (TI) and mechanical index (MI). Even if the irradiating ultrasound intensity remains at a permissible value, a higher-frequency ultrasound causes a higher TI. On the other hand, a lower-frequency ultrasound induces a higher MI. Therefore, T-beam frequency is selected to be 500 kHz under the condition of TI < 2 at a suitable acoustic intensity less than the maximum regulation level for the diagnostic ultrasound equipment, and MI < 0.25 that is less than one quarter of the cavitation threshold of MI $= 1$. D-beam frequency was selected to be 2 MHz, which is often used for TCD and transcranial color flow imaging (TCCFI) to observe the recanalization conditions. The system irradiates both T- and D-beams alternately controlled by the signal control sub-system through a common single aperture of the T/D compound probe, which includes two laminated phased array transducer elements for the T- and D-beams.

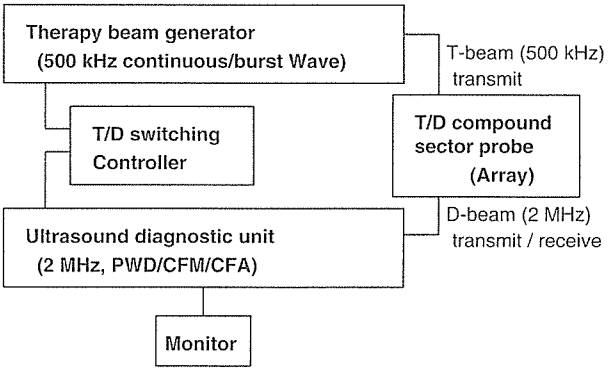

Fig. 1. Architecture of system.

2.2 *T/D compound probe*

The T/D compound probe, developed for thrombo embolic treatment with t-PA, has therapeutic and diagnostic